Emergence of localized patterns in globally coupled networks of relaxation oscillators with heterogeneous connectivity

Randolph J. Leiser[1] and Horacio G. Rotstein[1,2,*]

[1]*Department of Mathematical Sciences, New Jersey Institute of Technology, Newark, New Jersey 07102, USA*

[2]*Institute for Brain and Neuroscience Research, New Jersey Institute of Technology, Newark, New Jersey 07102, USA*

(Received 16 January 2017; published 3 August 2017)

Oscillations in far-from-equilibrium systems (e.g., chemical, biochemical, biological) are generated by the nonlinear interplay of positive and negative feedback effects operating at different time scales. Relaxation oscillations emerge when the time scales between the activators and the inhibitors are well separated. In addition to the large-amplitude oscillations (LAOs) or relaxation type, these systems exhibit small-amplitude oscillations (SAOs) as well as abrupt transitions between them (canard phenomenon). Localized cluster patterns in networks of relaxation oscillators consist of one cluster oscillating in the LAO regime or exhibiting mixed-mode oscillations (LAOs interspersed with SAOs), while the other oscillates in the SAO regime. Because the individual oscillators are monostable, localized patterns are a network phenomenon that involves the interplay of the connectivity and the intrinsic dynamic properties of the individual nodes. Motivated by experimental and theoretical results on the Belousov-Zhabotinsky reaction, we investigate the mechanisms underlying the generation of localized patterns in globally coupled networks of piecewise-linear relaxation oscillators where the global feedback term affects the rate of change of the activator (fast variable) and depends on the weighted sum of the inhibitor (slow variable) at any given time. We also investigate whether these patterns are affected by the presence of a diffusive type of coupling whose synchronizing effects compete with the symmetry-breaking global feedback effects.

DOI: 10.1103/PhysRevE.96.022303

I. INTRODUCTION

Several far-from-equilibrium chemical, biochemical, and biological systems exhibit oscillatory temporal patterns [1–7]. These phenomena are generated by the nonlinear interplay of positive and negative feedback effects operating at different time scales. Point (single) oscillators require at least one variable (activator) that favors both changes in its own production via autocatalytic effects and the production of a second variable (inhibitor). Inhibitors oppose changes in the activator on a slower time scale. Activators and inhibitors represent different state variables in different systems. Examples are the chemical compounds in the Belousov-Zhabotinsky reaction [8,9], the substrates and products in product-activated glycolytic oscillations [4,10], the activators and repressors in genetic oscillators, and the neuronal voltage and ionic current recovery variables [5].

In many realistic systems the time scales between activators and inhibitors are well separated, and the resulting oscillations are of the relaxation type [2,5]. These are captured by the prototypical van der Pol model for a triode circuit [11] and the FitzHugh-Nagumo (FHN) tunnel-diode model for nerve cells [12,13] and, also, by more detailed models such as the Oregonator for the Belousov-Zhabotinsky reaction [14–16], the Morris-Lecar model for neuronal oscillations [17], modified versions of the Selkov model for glycolytic oscillations [18–21], and genetic oscillators [22].

The complexity of individual relaxation oscillators results from the combined effect of two distinct inherent properties: (i) the presence of characteristic types of nonlinearities (typically cubiclike) and (ii) the time-scale separation between the participating variables referred to above. In addition to the typical large-amplitude oscillations (LAOs) of the relaxation type, these systems may exhibit small-amplitude oscillations (SAOs), with an amplitude difference of roughly an order of magnitude between LAOs and SAOs, as well as abrupt transitions between them (canard phenomenon) as a control parameter changes through a critical range (exponentially small in the parameter defining the slow time scale) [23–29]. Individual two-dimensional (2D) relaxation oscillators may display either SAOs or LAOs, but not both. Higher dimensional relaxation oscillators may exhibit mixed-mode oscillations (MMOs) [30,31], where LAOs are interspersed with SAOs. This creates additional effective time scales.

In addition to the individual oscillators' intrinsic feedback effects, oscillatory networks have feedback effects that result from the interplay of the connectivity and the intrinsic properties of the individual oscillators. The effects of global coupling, where each oscillator in the network is affected by the dynamics of the whole, have been studied in a variety of systems both experimentally and theoretically. These include oscillatory chemical reactions [32–37], electrochemical oscillators [38–48], laser arrays [49], catalytic reactions [50], saltwater oscillators [51], metabolic oscillators and cellular dynamics [20,52,53], cardiac oscillators [54,55], coupling through quorum sensing [56–60], circadian oscillators [61–63], neuronal networks [5,64–69], and image processing [65,70].

Globally coupled networks of 2D relaxation oscillators have been shown to generate oscillatory cluster patterns [20,32–35,38,39,64,71–75] where each cluster consists of synchronized in-phase identical oscillators. Oscillators in different clusters differ in at least one of their attributes (e.g., frequency, amplitude, or phase). Typical examples are the phase-locked (e.g., antiphase) oscillatory two-cluster patterns where each cluster exhibits LAOs or MMOs. The latter typically reflect the effects of the network connectivity (e.g., inhibition transiently

*horacio@njit.edu

pushing the activator down or terminating an oscillation before it reaches high enough values) and/or the interaction between the connectivity and the intrinsic canard structure [76] of the individual oscillators [72,73].

A more complex type of pattern that emerges in these globally coupled networks is localized oscillations, where one cluster exhibits LAO or MMOs and the other shows no oscillations or SAOs [32–36,72,73]. The break of symmetry requires some type of network heterogeneity such as different cluster sizes or different global feedback intensities acting on each cluster. Because the individual oscillators are monostable (SAOs or LAOs but not both), localized patterns are a network phenomenon that involves the interplay of the connectivity and the intrinsic dynamic properties of the individual nodes. In previous work, we showed that the canard phenomenon (generated in a supercritical Hopf bifurcation) present in individual oscillators plays an important role in the generation of localized patterns. However, the dynamic mechanisms that give rise to localized oscillatory patterns in networks of relaxation oscillators and how these patterns depend on the properties of the participating oscillators are not fully understood.

The goal of this paper is to address these issues in the context of globally coupled networks where the global feedback term affects the rate of change of the activator (fast variable) and depends on the weighted sum of the inhibitor (slow variable) at any given time [32–36,72,73]. An additional goal is to understand how these patterns are affected by the presence of a diffusive type of coupling. Since, in contrast to global inhibition, diffusion tends to synchronize oscillators, their interplay generates a competition between the two opposing effects.

We use a cluster reduction of dimensions argument [35] and assume that the system is divided into two clusters of the same or different sizes. The effects of the cluster size on the dynamics of these two-cluster networks are absorbed into the global feedback parameter coding for the intensity. Different cluster sizes result in an effective heterogeneous connectivity.

To capture the intrinsic dynamics of the individual oscillators we use a piecewise-linear (PWL) relaxation oscillator model of the FitzHugh-Nagumo type, which is an extension of the one we used in [77] to investigate the mechanisms of generation of the canard phenomenon. PWL models can be explicitly analyzed using linear tools of dynamical systems and matching "pieces of solutions" corresponding to consecutive linear regimes. PWL models have been used in a variety of fields as caricatures of nonlinear models to provide insights into the dynamics of smooth nonlinear models to investigate the dynamics of either individual nodes or individual networks [78–104].

As in [77], the activator (v) nullcline we use is cubiclike and has four linear pieces (Fig. 1; red curve). The inhibitor (w) nullcline is sigmoidlike and has three linear pieces (Fig. 1; green curve). The canard phenomenon requires the presence of the two linear pieces in the middle branch of the v-nullcline but a linear piece for w-nullcline suffices [77]. However, localization in models having a linear w-nullcline is more difficult to obtain and is less robust than in models having sigmoidlike w-nullclines. In addition, the realistic models mentioned above have inhibitor nullclines of the sigmoid type.

An additional advantage of using PWL models for this study is that they provide a way of understanding how the

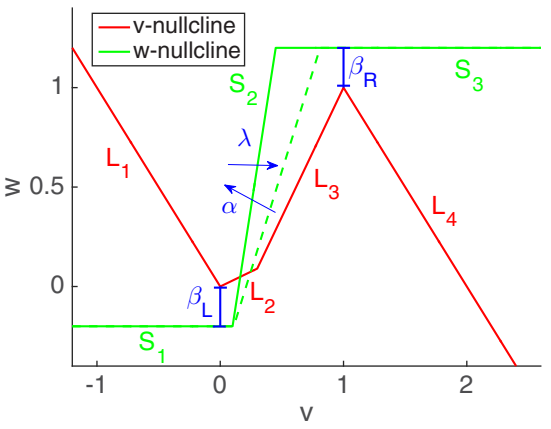

FIG. 1. Cubic- and sigmoidlike piecewise linear v- and w-nullclines for system (1). The v-nullcline $f(v)$ (red line) is given by (2). We used the parameter values $\eta = 0.3$ and $v_c = 0.3$. The w-nullcline $g(v;\lambda)$ (green lines) is given by (3). We used the following parameter values for the two superimposed w-nullclines: $\alpha = 4$ (solid green line), $\alpha = 2$ (dashed green line), $\lambda = 0.3$ (solid green line), $\lambda = 0.21$ (dashed green line), $\beta_L = \beta_R = 0.2$. Arrows indicate the effects of increasing values of λ and α. Increasing (decreasing) λ displaces the w-nullcline to the right (left), while increasing (decreasing) α increases (decreases) the slope of the w-nullcline.

intrinsic properties of the individual oscillators affect the network dynamics in terms of the different linear portions of the PWL nullclines whose properties are easily captured by their slopes, endpoints, and other parameters. For example, with an increase in the values of β_L and β_R in Fig. 1 the w-nullcline becomes "more linear" in the region of the phase plane where the oscillations occur (around the four branches of the cubiclike v-nullcline). This allows us to compare the effects of the different "degrees of nonlinearity" in terms of the parameters β_L and β_R. In this paper we compare two representative scenarios, where the w-nullcline is sigmoidlike, as in Fig. 1 ($\beta_L = \beta_R = 0.05$), and linearlike, with both β_L and β_R significantly larger ($\beta_L = \beta_R = 1$).

The localized patterns as well as the other types of MMO patterns analyzed in this paper can be a desired or an undesired result of the network activity. For memory devices and working memory [105–108], localized patterns allow for the effective representation of information in the LAO components. In contrast, the presence of localized oscillations may disrupt the communication between neurons [5] and the effective pulsatile secretion of insulin when controlled by glycolytic oscillators or other oscillatory systems (e.g., calcium) [20,109–111] (but see [112]). Our results will contribute to the understanding of the mechanisms underlying the generation of these patterns and how to control or prevent them when necessary.

The outline of the paper is as follows. Methods are reported in Sec. II. In Sec. III A we discuss the occurrence of the canard phenomenon for individual oscillators. This is an extension of previous work [77] for linear w-nullclines. In Sec. III B we discuss the canard phenomenon induced by the global feedback parameter (γ) when the system exhibits bulk oscillations (one cluster). As γ increases, the LAOs abruptly transition to SAOs. Globally coupled bulk oscillations are not likely to be a realistic scenario, but it is a useful

step towards the investigation of two-cluster systems. The main reason is that the interaction between mutually coupled oscillators can be understood in terms of a dual contribution of the coupling term: (i) the modification of the dynamic structure of the autonomous part of each individual oscillator and (ii) a forcing exerted on each oscillator by the others. The latter may favor, disrupt, or interfere with the canard phenomenon. In Secs. III C and III D we characterize the different network patterns that emerge in the globally coupled system with different cluster sizes (heterogeneous), including phase-locked LAOs, MMOs, and localized patterns. Cluster patterns with the same cluster size show phase-locked LAOs but not localized patterns. In Secs. III E and III F we explore the transition mechanisms from phase-locked to localized patterns as γ increases. This transition is abrupt for models with sigmoidlike nullclines but gradual for models with linearlike nullclines. In Sec. III G we show that the oscillation frequency of the localized patterns in the two types of models have different monotonic dependencies on γ. In Secs. III H to III J we explore additional dynamic differences between the two types of models. In Sec. IV we discuss our results and their limitations and implications for network dynamics. Results on the dynamics of linear regimes are provided in Appendix A. Finally, in Appendix B we explore how the interplay of global and diffusive (local) coupling between clusters affects the generation of localized clusters. While this is not a realistic situation, since diffusive coupling occurs between oscillators and not between clusters, it allows us to explore the interplay of two competing effects: the tendency of global coupling to create clusters and the tendency of diffusion to synchronized oscillators.

II. METHODS

A. Piecewise linear models of the FitzHugh-Nagumo type

We consider the following PWL model of the FHN type:

$$\begin{aligned} v' &= f(v) - w, \\ w' &= \epsilon\,[\,g(v;\lambda) - w\,], \end{aligned} \tag{1}$$

where the prime sign represents the derivative with respect to the variable t and the functions f and g are PWL cubic- and sigmoidlike functions (see Fig. 1) given, respectively, by

$$f(v) = \begin{cases} -v & \text{if } v < 0, \\ \eta\, v & \text{if } 0 \leqslant v < v_c, \\ (1-\eta\, v_c)/(1-v_c)\,(v-1)+1 & \text{if } v_c \leqslant v \leqslant 1, \\ -v+2 & \text{if } 1 \leqslant v \end{cases} \tag{2}$$

and

$$g(v;\lambda) = \begin{cases} -\beta_L & \text{if } v < (\lambda-\beta_L)/\alpha, \\ \alpha\, v - \lambda & \text{if } (\lambda-\beta_L)/\alpha \leqslant v \leqslant (\lambda+1+\beta_R)/\alpha, \\ 1+\beta_R & \text{if } v > (\lambda+1+\beta_R)/\alpha. \end{cases} \tag{3}$$

The PWL cubiclike function f (Fig. 1; red line) has a minimum at (0,0) and a maximum at (1,1). As in the smooth case, this choice ensures that large-amplitude oscillations are $\mathcal{O}(1)$ [77]. The parameter η governs the slopes of the two middle branches L_2 and L_3. The slope of L_3 also depends on the parameter v_c (v coordinate of the point joining L_2 and L_3). The slopes of both the left (L_1) and the right (L_4) branches are equal to -1.

The PWL sigmoid function g (Fig. 1; green line) has three branches. The two horizontal branches S_1 and S_3 are below and above the minimum and maximum of f, respectively. The middle branch S_2 joins these two horizontal branches. The parameter λ controls the displacement of g to the right ($\lambda > 0$) or the left ($\lambda < 0$). The parameter α controls the slope of the middle branch S_2, which increases with increasing values of α. In the limit of $\beta_L, \beta_R \to \infty$, the PWL system is the one used in [77], where g is a linear function.

B. Linear regimes and virtual fixed-points

The dynamics of a PWL model of the form of (1)–(3) can be divided into four linear regimes R_k ($k = 1, \ldots, 4$), corresponding to the four linear pieces L_k of the cubiclike PWL function $f(v)$ (Fig. 2). The initial conditions in each regime are equal to the values of the variables v and w at the end of the previous regime where the trajectory has evolved.

In each linear regime the dynamics are organized around a virtual fixed point (Fig. 2), which results from the intersection between the w-nullcline (green line) and the corresponding linear piece (red line) or its extension beyond the boundaries of this regime (dashed red line). In the latter case the virtual fixed points do not coincide with the actual fixed points, and are located outside the corresponding regime, but still play an important role in determining the dynamics in that regime. The trajectories in a given regime never reach the purely virtual stable fixed points (outside the regime), but their presence provides information on the trajectory's direction of motion. More specifically, within the boundaries of each regime trajectories evolve according to the linear dynamics defined in that regime as if the dynamics were globally linear, and they "do not feel" that the "rules" governing their evolution will change at a future time when the trajectory moves to a different regime. We refer the reader to [77] for more details.

C. Networks of PWL oscillators with global inhibitory feedback

We consider networks of PWL oscillators of the FHN type and the form of (1) globally coupled through the inhibitor variable (w),

$$\begin{aligned} v_k' &= f(v_k) - w_k - \gamma\,\Gamma(\mathbf{w}), \\ w_k' &= \epsilon\,[\,g(v_k;\lambda) - w_k\,], \end{aligned} \tag{4}$$

for $k = 1, \ldots, N$, where N is the total number of oscillators in the network, $\gamma \geqslant 0$ is the global feedback parameter, and

$$\Gamma(\mathbf{w}) = \frac{1}{N}\sum_{k=1}^{N} w_k. \tag{5}$$

D. Cluster reduction of dimensions and heterogeneous coupling

Following previous work [35,36,72,73] we assume that the network is divided into two clusters where all oscillators in each cluster are identical and have identical dynamics, while

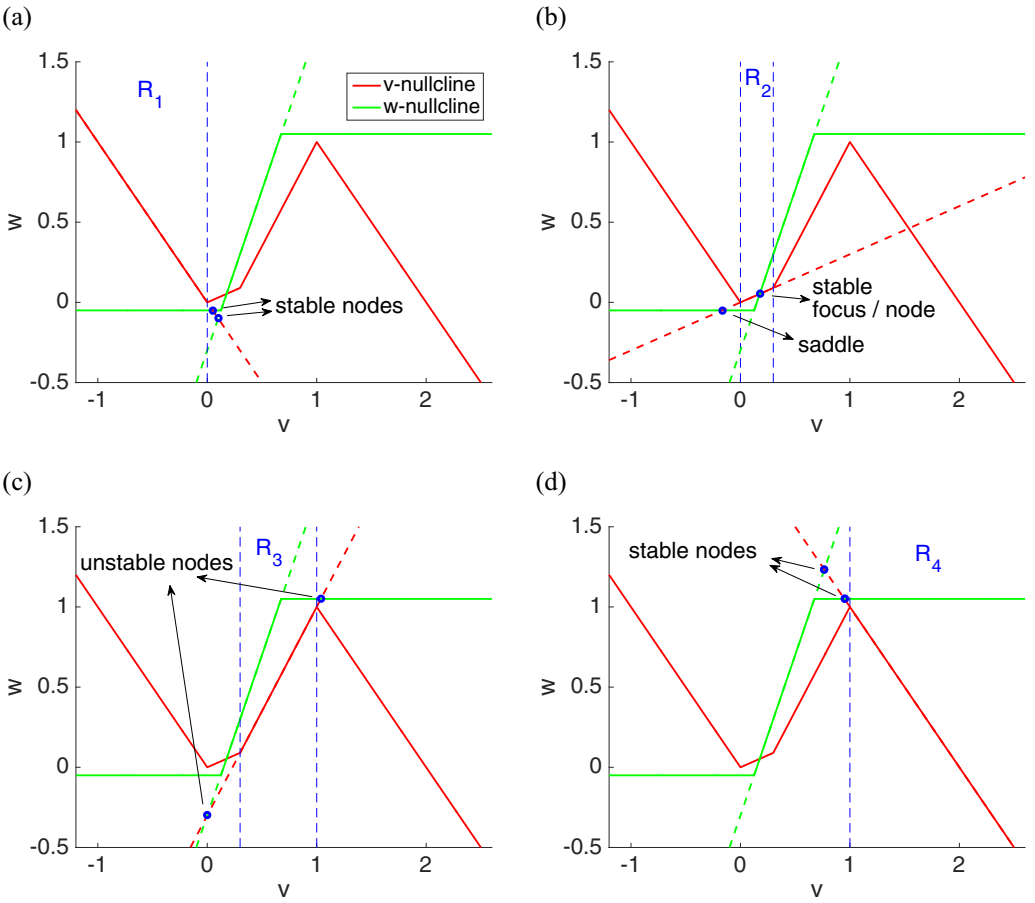

FIG. 2. Linear regimes and actual and virtual fixed points for system (1). The v-nullcline (red lines) is as in Fig. 1. For the w-nullcline (green lines) we used $\alpha = 2, \lambda = 0.3, \beta_L = \beta_R = 0.05$. The superimposed dashed green w-nullcline is linear (extension of the linear piece S_2). The virtual fixed points for each regime (small blue circles) are the intersections between the extensions of the corresponding linear pieces and the w-nullcline. The stable virtual fixed point for R_2 coincides with the actual fixed point.

oscillators in different clusters may have different dynamics. Accordingly, for a two-cluster network,

$$\Gamma(\mathbf{w}) = \sigma_1 w_1 + \sigma_2 w_2, \tag{6}$$

where σ_1 and σ_2 ($\sigma_1 + \sigma_2 = 1$) are the fractions of oscillators in each cluster. Alternatively, the global coupling term, (6), can also be interpreted as consisting of clusters with the same fraction of oscillators each, but heterogeneous connectivity.

System (4) with (6) can be written as

$$\begin{aligned} v_k' &= f(v_k) - (1 + \sigma_k\, \gamma)\, w_k - \sigma_j\, \gamma\, w_j, \\ w_k' &= \epsilon\, [\, g(v_k; \lambda) - w_k\,] \end{aligned} \tag{7}$$

for $k, j = 1,2$ with $j \neq k$. The zero-level surfaces ("higher-dimensional nullclines") for the kth oscillator are given by

$$w_k = N_{v,k}(v_k, w_j; \gamma) = \frac{f(v_k)}{1 + \sigma_k \gamma} - \frac{\gamma\, \sigma_j w_j}{1 + \sigma_k \gamma}, \quad k, j = 1,2, \quad j \neq k, \tag{8}$$

and

$$w_k = N_{w,k}(v) = g(v; \lambda), \quad k = 1,2, \tag{9}$$

respectively.

Equation (8) describes a 2D surface having the shape of the first term on the right-hand side of $N_{v,k}(v_k, 0; \gamma)$. For $\gamma > 0$, we view the nullsurface, (8), as the v-nullcline for the individual (uncoupled) oscillator $N_{v,k}(v, 0; 0)$, flattened by the effect of the denominator and forced by the second oscillator via the variable $w_j(t)$. When there is no ambiguity, we refer to the autonomous part $N_{v,k}(v_k, 0; \gamma)$ in (8) as the v-nullcline for the oscillator O_k. The oscillations in the latter "raise" and "lower" this v-nullcline following the dynamics of w_j and therefore affect the evolution of the trajectories in the phase-plane diagrams.

E. Diffusive coupling between clusters

System (7) with an added diffusion term reads

$$\begin{aligned} v_k' &= f(v_k) - (1 + \sigma_k\, \gamma)\, w_k - \sigma_j\, \gamma\, w_j + D_v\, (v_j - v_k), \\ w_k' &= \epsilon\, [\, g(v_k; \lambda) - w_k\,] \end{aligned} \tag{10}$$

for $k, j = 1,2$ with $j \neq k$, where D_v is the diffusion coefficient. This way of adding diffusion is somehow artificial and does not reflect the diffusive effects in the original system, nor is it derived from it. However, its inclusion helps to clarify the competitive effects of global inhibition and diffusion.

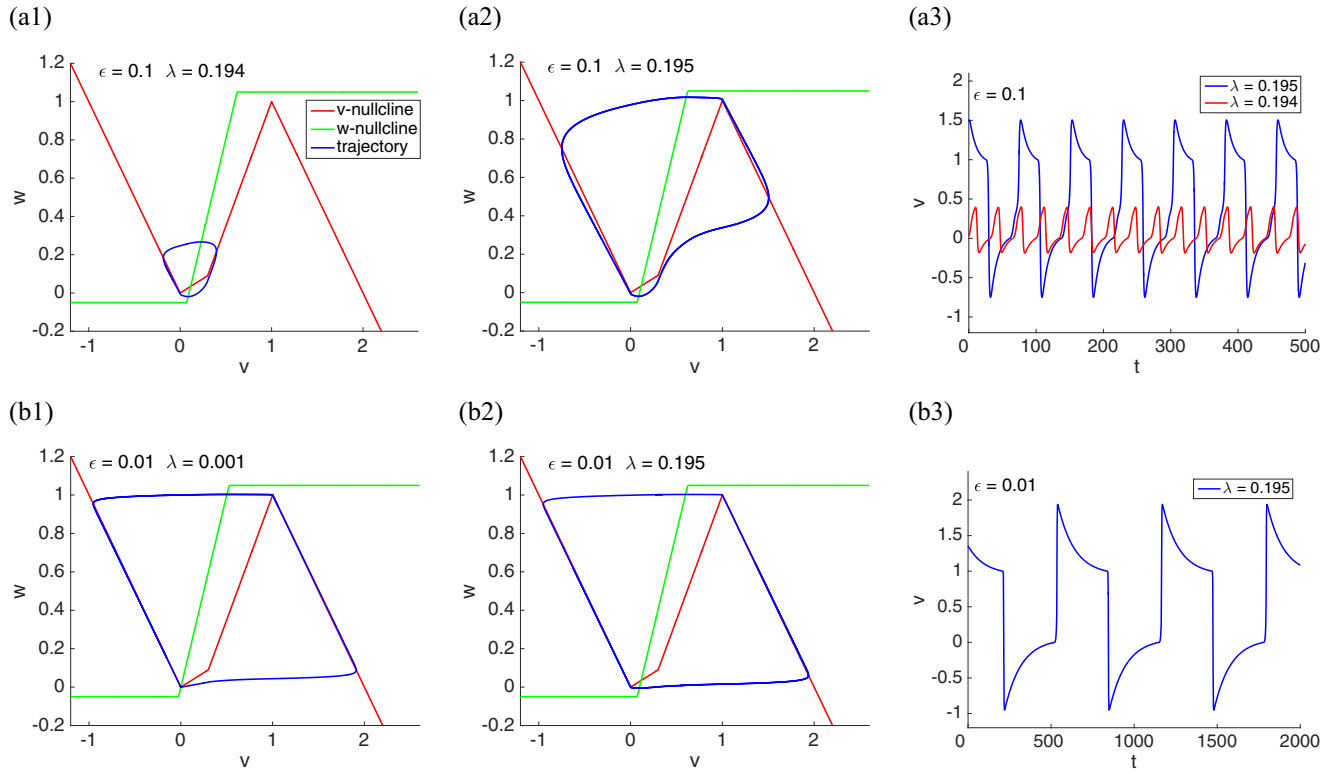

FIG. 3. Dynamics of system (1) for representative parameter values. The v- and w-nullclines are as in Fig. 1. (a) Canard phenomenon as λ crosses $\lambda_c \in (0.194, 0.195)$. The actual fixed points are foci. (b) The actual fixed points are nodes (no SAOs).

Equation (8) is extended to

$$w_k = N_{v,k}(v_k, v_j, w_j; \gamma, D_v) = \frac{f(v_k) - D_v\, v_k}{1 + \sigma_k \gamma} - \frac{\gamma\, \sigma_j w_j - D_v\, v_j}{1 + \sigma_k \gamma}, \quad k, j = 1,2, \;\; j \neq k. \tag{11}$$

For $D_v > 0$ the v-nullcline $N_{v,k}(v_k, 0, 0; \gamma, D_v)$ is linearly modified by the term $D_v\, v_k$. In contrast to global coupling, this effect is not homogeneous for all values of v_k but is dependent on its sign. For positive values of v_k the v-nullcline is flattened, while for negative values of v_k the v-nullcline is sharpened. The oscillations in v_j raise and lower this v-nullcline following its dynamics. In order for the linear piece L_2 to remain positive for $D_v > 0$, we restrict $D_v < \eta$.

F. Numerical simulations

Numerical solutions were computed using the modified Euler method (Runge-Kutta, order 2) [113] with a time step $\Delta t = 0.1$ ms (or smaller values of Δt when necessary) in MATLAB (The Mathworks, Natick, MA).

III. RESULTS

A. The canard phenomenon for PWL models of the FHN type revisited

In a 2D relaxation oscillator, the canard phenomenon refers to the abrupt transition between SAOs and LAOs as a control parameter crosses a very small critical range [Figs. 3(a)], which is exponentially small in the parameter defining the slow time scale (ϵ) [23–29]. We identify this critical range with a critical value for the control parameter (e.g., λ_c if the control parameter is λ). If the Hopf bifurcation underlying the creation of the SAOs is supercritical (subcritical), then the SAOs are stable (unstable). Relaxation-type LAOs are always stable.

The canard phenomenon for PWL models of the FHN type with a linear w-nullcline has been described in [7] and [98] and has been throughly analyzed in [77]. Here we briefly describe it in the context of the PWL models of the FHN type with sigmoidlike PWL w-nullclines using the parameter λ as the control parameter (Fig. 3).

For the SAOs to be generated [Fig. 3(a1)], the limit cycle must cross either the linear piece L_2 or the first portion of the linear piece L_3 of the v-nullcline. Otherwise [Fig. 3(a2)] the limit cycle trajectory moves into the linear regime R_4 and the system displays LAOs. For a trajectory arriving in R_2 to be able to cross L_2 or the first portion of L_3, the actual fixed point in R_2 must be a focus [see Eq. (A4) with $\kappa = 1$ in Appendix A]. In addition, the initial amplitude of the trajectory in R_2 (the distance between the actual fixed point and the initial point in R_2) must be small enough so that the trajectory reaches the v-nullcline before reaching the region of fast motion, which would cause it to move towards the right branch. For the parameter values in Figs. 3(a), $|\eta + \epsilon| = 0.4$ and $2\sqrt{\epsilon\,\alpha} \sim 0.89$ in the linear regime R_2 and therefore the actual fixed point is a focus (Appendix A). However, as ϵ decreases this inequality may no longer hold. For example, for the parameters in Figs. 3(b), $|\eta + \epsilon| = 31$ and $2\sqrt{\epsilon\,\alpha} \sim 0.28$, and therefore the actual fixed point is a node (see Appendix A), and as a consequence, the system is no longer able to exhibit the canard phenomenon.

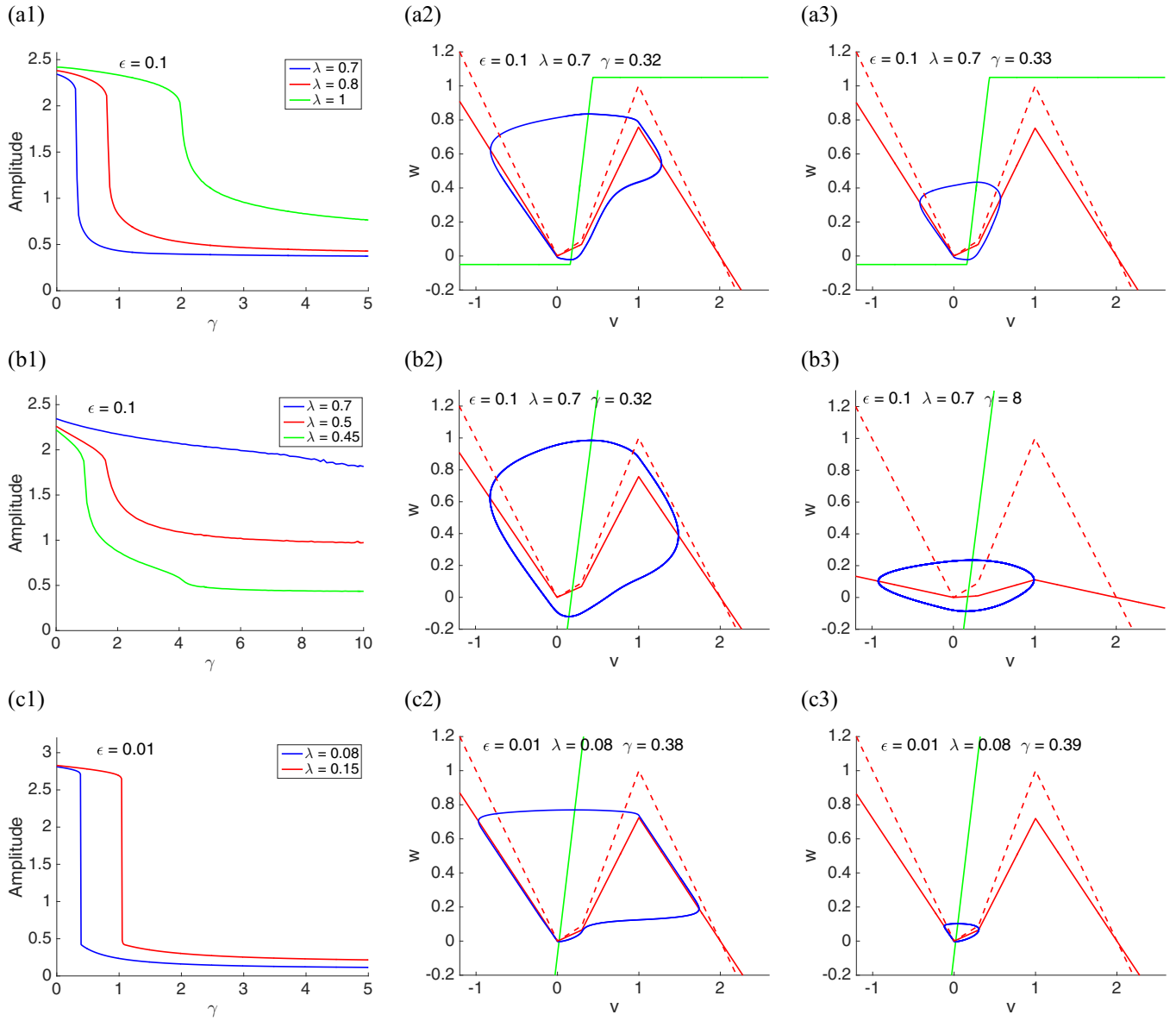

FIG. 4. The canard phenomenon induced by global inhibitory feedback in bulk (one-cluster) oscillatory systems. The solid red v-nullclines in the phase-plane diagrams (middle and right columns) correspond to the actual values of γ used in each panel. The v-nullcline for $\gamma = 0$ (dashed red line in phase-plane diagrams) is as in Fig. 1 and is presented for reference. For the w-nullcline we used the following parameter values: (a) $\alpha = 4, \epsilon = 0.1, \lambda = 0.7, \beta_L = \beta_R = 0.05$; (b) $\alpha = 4, \epsilon = 0.1, \lambda = 0.7, \beta_L = \beta_R = 1$; (c) $\alpha = 4, \epsilon = 0.01, \lambda = 0.08, \beta_L = \beta_R = 1$.

The canard critical value λ_c is affected by the vector field away from the local vicinity of the small-amplitude limit cycle. For example, all other parameters equal, for linearlike w-nullclines, when the horizontal pieces are far away from the v-nullcline (e.g., $\beta_L = \beta_R = 1$), λ_c is smaller than for the parameters in Figs. 3(a) (not shown). Additionally, the oscillation frequencies for values of λ around λ_c are larger for linearlike than for sigmoidlike w-nullclines.

B. The canard phenomenon induced by global feedback

Here we follow previous work [35,36,73] and focus on the dynamics of the one-cluster globally coupled system, (7): $\sigma_1 = 1$ ($\sigma_2 = 0$). This is not likely to be a realistic situation since one expects the network bulk oscillations to be unstable for sufficiently large values of the global feedback parameter γ and the network to be separated into clusters. However, the dynamics of this reduced system show how the canard phenomenon results from changes in γ for constant values of λ. The results in this section will be helpful in understanding the dynamics of the autonomous component of the two-cluster systems discussed later in this paper.

From (A4) in Appendix A with $\kappa = 1 + \gamma$, increasing values of γ (all other parameters fixed) can cause the fixed point to transition from a node to a focus. In addition, from (A2) in Appendix A, increasing values of γ change the location of the fixed point. Therefore, the global feedback parameter γ can act as a control parameter that induces the canard phenomenon for fixed values of λ (Fig. 4).

The left panels in Fig. 4 show curves of the oscillation amplitude versus γ for representative parameter values. The corresponding middle and right panels show the phase-plane

diagrams for values of γ before and after the canard phenomenon (for blue curves in the top panels). The parameter values in Figs. 4(a) and 4(b) are the same, except for the w-nullcline, which is sigmoidlike in Figs. 4(a) and linearlike in Figs. 4(b). The w-nullcline in Figs. 4(c) is linearlike [as in Figs. 4(b)], but ϵ is smaller than in Figs. 4(b) (larger time-scale separation).

In Figs. 4(a) the canard phenomenon is induced by changes in γ. The transition is more pronounced for lower values of λ. As γ increases, the v-nullcline flattens [Figs. 4(a2) and 4(a3)], and for γ_c the limit cycle trajectory is able to cross L_3, thus generating SAOs [Fig. 4(a3)] instead of moving towards R_4 to generate LAOs [Fig. 4(a2)].

For the same value of ϵ and the linearlike w-nullcline in Figs. 4(b), the system fails to exhibit the canard phenomenon as γ changes. The effective time-scale separation in the vicinity of the minimum of the v-nullcline is smaller than in Figs. 4(a) because of the absence of the horizontal piece of the w-nullcline [compare Figs. 4(a1) and 4(a2) with Figs. 4(b1) and 4(b2)], and therefore the limit-cycle trajectories are more

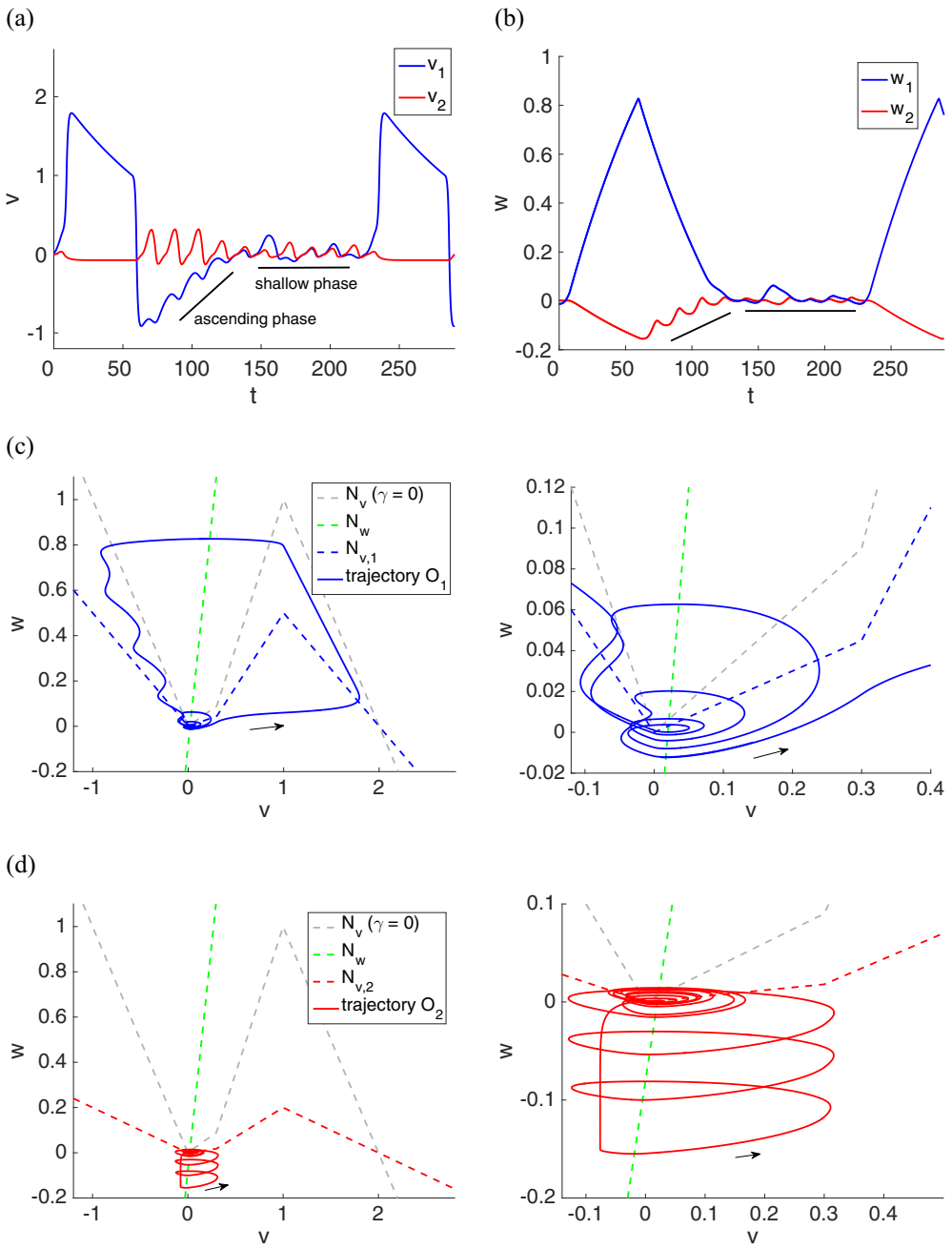

FIG. 5. Canard and noncanard (standard) SAOs in two-cluster networks. (a) Curves of v_1 and v_2 vs t. (b) Curves of w_1 and w_2 vs t. (c, d) Phase-plane diagrams. Dashed gray curves represent the v-nullcline for the uncoupled system ($\gamma = 0$). Dashed blue and red curves represent the v-nullclines for the autonomous part of the globally coupled system. Dashed green curves represent the w-nullclines. Solid blue and red curves represent the trajectories of the globally coupled system for the oscillators O_1 and O_2, respectively. Right panels are magnifications of left panels. We used the following parameter values: $\alpha = 4$, $\epsilon = 0.01$, $\lambda = 0.08$, $\sigma_1 = 0.2$, $\sigma_2 = 0.8$, $\gamma = 5$, and $\beta_L = \beta_R = 1$.

rounded in Figs. 4(b) than in Figs. 4(a). This causes the limit-cycle trajectory to move farther away from L_2 and L_3 in Fig. 4(b2) than in Fig. 4(a2). As a result, the v-nullcline is able to flatten significantly before the limit-cycle trajectory is able to cross the middle branch, and therefore the oscillations' amplitude decreases gradually instead of abruptly. For lower values of λ [red and green curves in Figs. 4(b)] the transition from LAOs to SAOs is faster and the final amplitude smaller than for $\lambda = 0.7$, but still this transition is not abrupt.

A decrease in ϵ for the same parameter values as in Figs. 4(b) restores the ability of γ to induce the canard phenomenon [Figs. 4(c)]. The decrease in ϵ compensates for the lack of the horizontal pieces of the w-nullcline, thus maintaining similar levels of the time-scale separation in the vicinity of the minimum of the v-nullcline.

As discussed in the previous section, for $\epsilon = 0.01$ and $\alpha = 2$ the uncoupled oscillator ($\gamma = 0$) fails to exhibit the canard phenomenon. However, the canard phenomenon can be induced by γ (not shown) with properties similar to those at $\alpha = 4$ in Figs. 4(c). The values of γ_c increase with λ, and in contrast to the $\alpha = 4$ case, they are both significantly larger for $\alpha = 2$ than for $\alpha = 4$. Also, the range of values of γ_c spanned by λ is significantly larger for $\alpha = 2$ than for $\alpha = 4$.

C. Canard and noncanard (standard) SAOs for two interacting oscillators forcing one another

The interaction between two oscillators due to global coupling can be thought of as the two oscillators' forcing one another through the last term in the first equation in (7) as discussed above. If the product $\sigma_k\gamma$ ($k = 1,2$) is large enough, then the autonomous part of $N_{v,k}$, (8), can be in an SAO regime. This means that if w_j ($j = 1,2$ with $j \neq k$) were artificially made equal to 0, then the oscillator O_k would exhibit the type of canardlike SAOs discussed in the previous section. However, since w_j is not necessarily equal to 0 or very small, but also oscillates, $N_{v,k}$ increases and shifts down from its baseline location in an oscillatory fashion. This interferes with the canard SAOs to create the more complex patterns that we discuss in the following sections.

Among these patterns are the representative "blue" MMOs shown in Fig. 5(a), which consist of two types of SAOs. The ones along the ascending phase correspond to the portion of the trajectory evolving along the left branch of $N_{v,1}$ [Fig. 5(c)] as they respond to the motion of $N_{v,1}$ following the forcing exerted by O_2 [Fig. 5(d)]. Those in the more shallow phase correspond to the trajectories moving around the minimum of $N_{v,1}$, as they are able to cross the linear piece L_2 to create SAOs. We refer to them as canardlike SAOs.

Canardlike and standard SAOs are created by different mechanisms. The standard SAOs in v_1 [Fig. 5(a); blue line] primarily respond to the oscillatory input from w_2 [Fig. 5(b); red line]. During the ascending phase, w_1 is decreasing, therefore the oscillations in v_2 and w_2 are intrinsically generated by a canardlike mechanism [Fig. 5(d)] that does not require oscillations in the input. Canardlike SAOs are created by the canardlike mechanism described in the previous sections. Note that although v_1 receives an oscillatory input from w_2, the oscillations in w_2 have a smaller amplitude during the shallow phase than during the ascending phase, indicating that they are less important in the generation of the SAOs in O_1.

D. Localized, mixed-mode, phase-locked, and SAO network oscillatory patterns

In the next sections we examine the consequences of the global feedback's ability to induce the canard phenomenon in autonomous oscillators ($\sigma_1 = 1$ and $\sigma_2 = 0$) for two-cluster network dynamics ($\sigma_1 > 0$, $\sigma_2 > 0$). We use $\sigma_1 = 0.2$ ($\sigma_2 = 0.8$) as a representative case of heterogeneous clusters. Homogeneous clusters ($\sigma_1 = \sigma_2 = 0.5$) produce relatively simple network patterns as we briefly explain below.

From Eq. (7), the autonomous part of each oscillator is affected by both the cluster size (σ_k) and γ. In the absence of the forcing exerted by the other oscillator (w_j), the canard phenomenon in each oscillator would be induced by increasing values of both σ_k and γ [35,36]. The global feedback parameter critical value for the autonomous part of each oscillatory cluster is given by

$$\gamma_{c,k} = \frac{\gamma_c}{\sigma_k}, \tag{12}$$

where γ_c is the global feedback parameter critical value for the single-cluster oscillator discussed above [e.g., $\gamma_c = 0.32$ in Figs. 4(a) and $\gamma_c = 0.38$ in Figs. 4(c)].

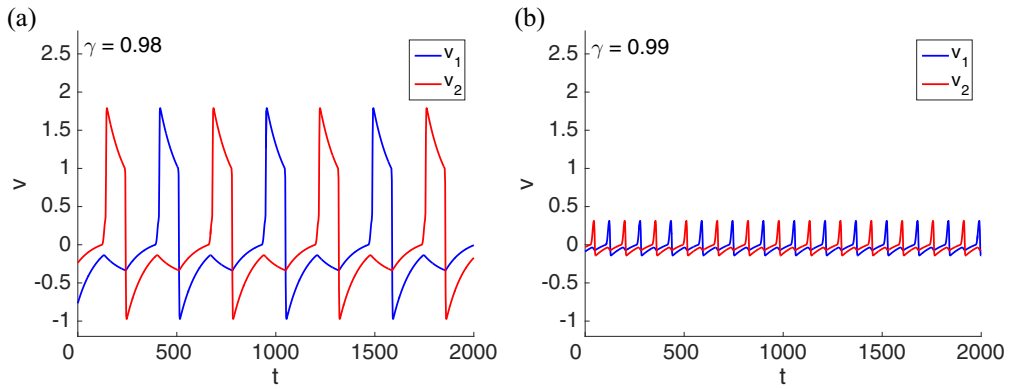

FIG. 6. Abrupt transition between antiphase LAO and antiphase SAO patterns in two-cluster networks for representative values of γ. Parameter values ($\alpha = 4$, $\epsilon = 0.01$, $\lambda = 0.08$, and $\sigma_1 = \sigma_2 = 0.5$) are as in Figs. 4(c), except that $\beta_L = 0.05$ and $\beta_R = 0.05$ [as in Figs. 4(a) and 4(b)].

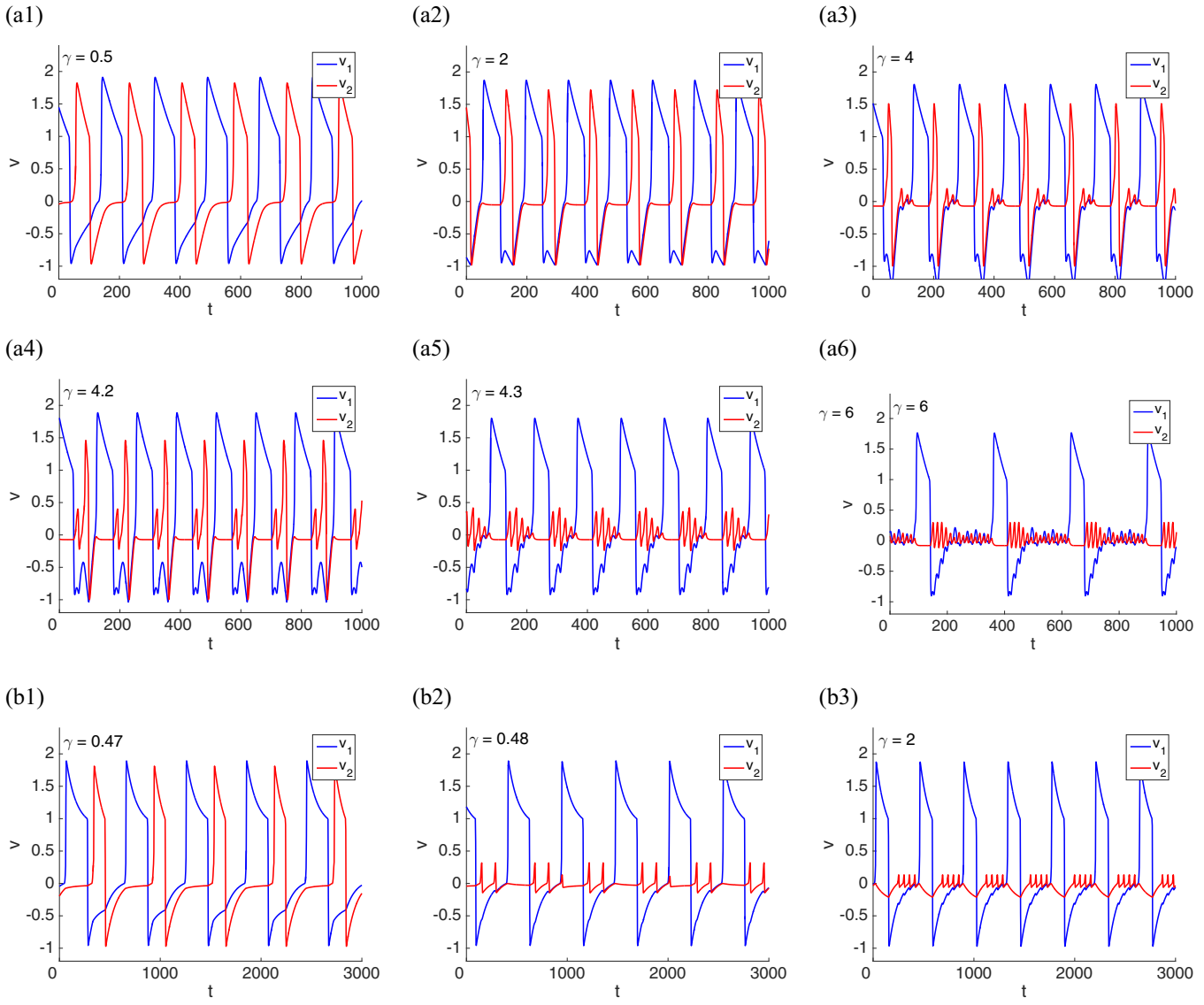

FIG. 7. Localization in a two-cluster network for representative values of γ. (a) Linearlike w-nullcline. Parameter values (see below) are as in Figs. 4(c) (including $\beta_L = \beta_R = 1$). (b) Sigmoidlike w-nullcline. Parameter values (see below) are as in Figs. 4(c), except that $\beta_L = \beta_R = 0.05$, which is the same as in Figs. 4(a) and 4(b). We used the following parameter values: $\alpha = 4$, $\epsilon = 0.01$, $\lambda = 0.08$, $\sigma_1 = 0.2$, and $\sigma_2 = 0.8$.

For $\sigma_1 = \sigma_2 = 0.5$, $\gamma_{c,1} = \gamma_{c,2}$, and therefore both oscillators would simultaneously be either in the LAO or in the SAO regime (Fig. 6), with no intermediate types of patterns. The forcing that the two oscillators exert on each other does not change this fact, but the values of γ at which these abrupt transitions occur are larger than the ones predicted by Eq. (12).

For example, for the parameter values in Fig. 6, $\gamma_{c,1} = \gamma_{c,2} \sim 0.72$ (not shown) and the transition occurs at $\gamma \sim 0.99$. For another example, for the same parameter values and $\beta_L = \beta_R = 1$ (a "more linear" w-nullcline), $\gamma_{c,1} = \gamma_{c,2} \sim 0.76$ [(see Figs. 4(c)] and the transition occurs at $\gamma \sim 5.21$ (not shown). In this case, the oscillation frequency is higher than in Fig. 6.

From Eq. (12), for $\sigma_1 \neq \sigma_2$ it is possible for one oscillator ($\sigma_1 < 0.5$) to be in the LAO regime, while the other ($\sigma_2 > 0.5$) is in the SAO regime, thus generating localized patterns (described in more detail below). However, the forcing effects that the oscillators exert on each other may disrupt this scenario and create more complex dynamics. It is, in fact, not *a priori* clear whether and under what conditions these localized patterns exist. For this to happen, the forcing effects should not interfere with the "autonomous" canard phenomenon for each oscillator. A richer repertoire of intermediate patterns that are not "purely LAO" or "purely SAO" is expected to result from the complex interactions between oscillators as happens for other systems [72,73].

We have identified various types of network patterns for different parameter regimes.

(i) Phase-locked LAO patterns [e.g., Figs. 7(a1) and 7(a2)] correspond to both oscillators in the LAO regime. All other parameters fixed, the phase difference between the two oscillators depends on the relative cluster sizes. For $\sigma_1 = \sigma_2 = 0.5$ the patterns are antiphase (Fig. 6). The underlying mechanisms are qualitatively similar to these described in [72] and [73]

involving the standard SAOs discussed above and are not discussed further in this paper.

(ii) Mixed-mode oscillatory patterns [e.g., Fig. 7(a3)] correspond to either one or both oscillators' exhibiting MMOs.

(iii) Localized patterns [e.g., Figs. 7(a5) and 7(a6) and Figs. 7(b2) and 7(b3)] correspond to one oscillator's exhibiting LAOs or MMOs, while the other exhibits exclusively SAOs. From Eq. (12), the oscillator with the larger cluster size is the one expected be in the SAO regime.

(iv) LAO localized patterns [e.g., Figs. 10(a3) and 10(b3)] correspond to the two oscillators' exhibiting LAOs or MMOs, but the number of LAOs per cycle's differing between the two oscillators. The typical situation is one oscillator's exhibiting one LAO per cycle, while the other exhibits a burst of LAOs.

(v) SAO patterns correspond to both oscillators' exhibiting SAOs, which may or may not be synchronized in phase or have the same amplitude.

In addition, we have identified various irregular patterns that emerge mostly as transition patterns between those mentioned above. We do not analyze these patterns in this paper.

E. Gradual transition from phase-locked LAO to localized patterns through network MMOs in the PWL model with a linearlike w-nullcline

Figures 7(a) show various representative two-cluster patterns for the same parameter values as in Figs. 4(c). The global feedback critical values are $\gamma_{c,1} \sim 1.9$ and $\gamma_{c,2} \sim 0.475$.

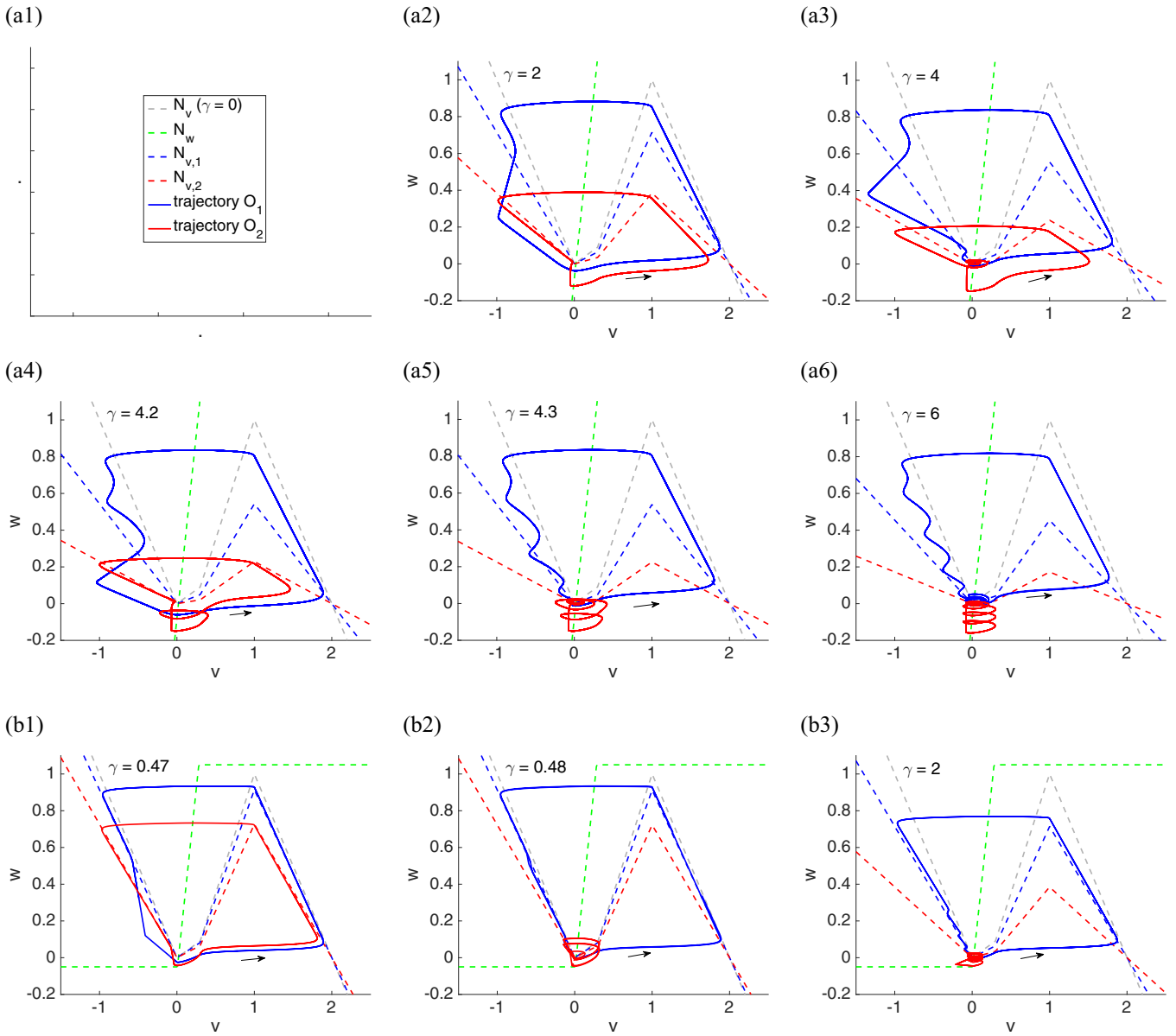

FIG. 8. Localization in a two-cluster network for representative values of γ. Phase-plane diagrams for the parameter values in Fig. 7. (a) Linearlike w-nullcline ($\beta_L = \beta_R = 1$). (b) Sigmoidlike w-nullcline ($\beta_L = \beta_R = 0.05$). Dashed gray curves represent the v-nullcline for the uncoupled system ($\gamma = 0$). Dashed blue and red curves represent the v-nullclines for the autonomous part of the globally coupled system. Dashed curves represent the w-nullclines. Solid blue and red curves represent the trajectories of the globally coupled system for the oscillators O_1 and O_2, respectively. We used the following parameter values: $\alpha = 4$, $\epsilon = 0.01$, $\lambda = 0.08$, $\sigma_1 = 0.2$, and $\sigma_2 = 0.8$.

The corresponding phase-plane diagrams are presented in Figs. 8(a).

For low values of γ [Figs. 7(a1) and 7(a2)], the system exhibits phase-locked LAO patterns. The duty cycle is smaller for the larger cluster (oscillator O_2) since its nullcline is flatter [Fig. 8(a2)]. The relative size of the (smaller to larger) duty cycles for the two oscillators O_1 and O_2 decreases with increasing values of γ.

As γ increases above these values, the system transitions to MMO patterns [Figs. 7(a3) and 7(a4)]. The SAOs for O_2 in Fig. 7(a3) are canardlike [Fig. 8(a3)] (the limit-cycle trajectories cross the linear piece L_2 or, at most, the early portion of L_3). The last SAO in each cycle for O_1 is also canardlike. They all occur, as both w_1 and w_2 are very small so their forcing effects are almost negligible. In contrast, the first SAOs in each cycle are standard (not canardlike) and reflect the motion of $N_{v,1}$ in response to the dynamics of O_2 as explained in Sec. III C.

During the active phase of O_1, O_2 is almost silent (constant). When O_1 jumps down, w_1 decreases and $N_{v,2}$ increases, thus releasing O_2. Because $N_{v,2}$ is flatter than $N_{v,1}$, O_2 completes the cycle just before O_1, and for some time they are both silent ($w_1 \sim 0$ and $w_2 \sim 0$). Figure 7(a4) corresponds to a slightly higher value of γ. This causes the first O_2 oscillation to transition to an SAO. As this happens, O_1 is moving along the left branch of $N_{v,1}$ and continuing to release O_2 from inhibition. As a result, the second O_2 oscillation is a LAO.

For larger values of γ, the system transitions to localized patterns [Figs. 7(a5) and 7(a6)] where the smaller cluster (O_1) exhibits MMOs and the larger cluster (O_2) exhibits canardlike SAOs [Figs. 8(a5) and 8(a6)]. The SAOs displayed by O_1 are a combination of canardlike and standard SAOs (as described above) in response to the dynamics of O_2. Note that the transition to localized patterns requires a value of γ much larger than the one predicted by $\gamma_{c,1}$ and $\gamma_{c,2}$.

F. Abrupt transition between phase-locked LAO and localized patterns for the PWL model with a sigmoidlike w-nullcline

Figures 7(b) show various representative two-cluster patterns for the same parameter values as in Figs. 7(a), but with a sigmoidlike w-nullcline. The corresponding phase-plane diagrams are presented in Figs. 8(b). The global feedback critical values are $\gamma_{c,1} \sim 1.8$ and $\gamma_{c,2} \sim 0.45$.

In contrast to Figs. 7(a), the transition from phase-locked SAO patterns [Fig. 7(b1)] to localized patterns [Fig. 7(b2)] is abrupt and occurs for a value of γ slightly higher than $\gamma_{c,2}$. This is the result of the stronger time-scale separation imposed by the sigmoidlike w-nullcline, particularly in the regions of the phase plane where the left and right branches of the v-nullcline are located [Figs. 8(b)].

When O_1 jumps up, it causes $N_{v,2}$ to shift down, thus inhibiting O_2. For the parameter values in Fig. 7(b1) (phase-locked SAO patterns), the trajectory for O_2 is above the minimum of $N_{v,2}$ and it continues to move down along $N_{v,2}$. After O_1 jumps down and begins to move down along $N_{v,1}$, decreasing the forcing exerted on O_2, it is released from inhibition and the trajectory moves through R_2 without crossing L_2, thus jumping up.

For the parameter values in Fig. 7(b2) (localized patterns) the trajectory for O_2 is almost at the minimum of $N_{v,2}$ when O_1 jumps up. The trajectory for O_2 first displays a small noncanard SAO, which is the result of O_1 causing $N_{v,2}$ to move down, and then two canard SAOs after O_1 jumps down and moves down along $N_{v,1}$. The larger value of γ increases the ability of the trajectory for O_2 to generate canardlike SAOs by crossing $N_{v,2}$ without jumping up.

The two models considered in this and the previous sections differ in the distances (β_L and β_R) between the horizontal pieces (S_1 and S_3) of the w-nullcline and the v-nullcline. To determine which one of β_L or β_R has a stronger effect in creating the abrupt transitions between the phase-locked LAO and the localized patterns described in this section, we looked at models with mixed values of these parameters. We found that for $\beta_L = 1$ and $\beta_R = 0.05$ the system behaves as in Figs. 7(a), while for $\beta_L = 0.05$ and $\beta_R = 1$ the system behaves as in Figs. 7(b). This confirms that the increase in the effective time-scale separation created by the left horizontal piece of the sigmoidlike w-nullcline is key for the results discussed above (and in the next section).

G. The oscillation frequency of the localized patterns in models with sigmoid- and linearlike w-nullclines has different monotonic dependencies on γ

Comparison of the localized patterns in Figs. 7(a5) and 7(a6) versus Figs. 7(b2) and 7(b3) shows that the LAO frequency of the oscillator O_1 decreases with increasing values of γ for the linearlike w-nullcline [Figs. 7(a5) and 7(a6)], while it increases with increasing values of γ for the sigmoidlike w-nullcline [Figs. 7(b2) and 7(b3)]. The underlying mechanisms in both cases involve the presence of canardlike SAOs. In Fig. 7(a5), O_1 jumps up right after reaching the minimum of $N_{v,1}$ [Fig. 8(a5)]. In Fig. 7(a6), O_1 engages in canardlike SAOs after reaching the minimum of $N_{v,1}$ [Fig. 8(a6)], thus increasing the LAO period. This is the result of the forcing exerted by O_2 and lower time-scale separation for the linearlike w-nullcline in Figs. 7(a) compared to the sigmoidlike w-nullcline in Figs. 7(b).

For the sigmoidlike w-nullcline [Figs. 7(b2) and 7(b3)], the number of SAOs per cycle also increases as γ increases. However, O_1 jumps up upon reaching the minimum of $N_{v,1}$. Also, more importantly, the number of cycles per unit of time increases with γ because the active phase of O_1 significantly decreases with increasing values of γ. This is the result of the flattening of the v-nullcline as γ increases and the fact that O_1 jumps down near the maximum of the baseline $N_{v,1}$.

H. Localized patterns persist for lower values of α for the PWL model with a sigmoidlike w-nullcline but not for a linearlike w-nullcline

From our previous discussion about the effects of decreasing values of α on the ability of λ and γ to induce the canard phenomenon in the uncoupled and coupled systems, respectively, it is not *a priori* clear whether the localized patterns found in the previous section for $\alpha = 4$ will persist when we decrease α. In Fig. 9 we present our results for the same parameter values as in Fig. 7 and $\alpha = 2$ (instead

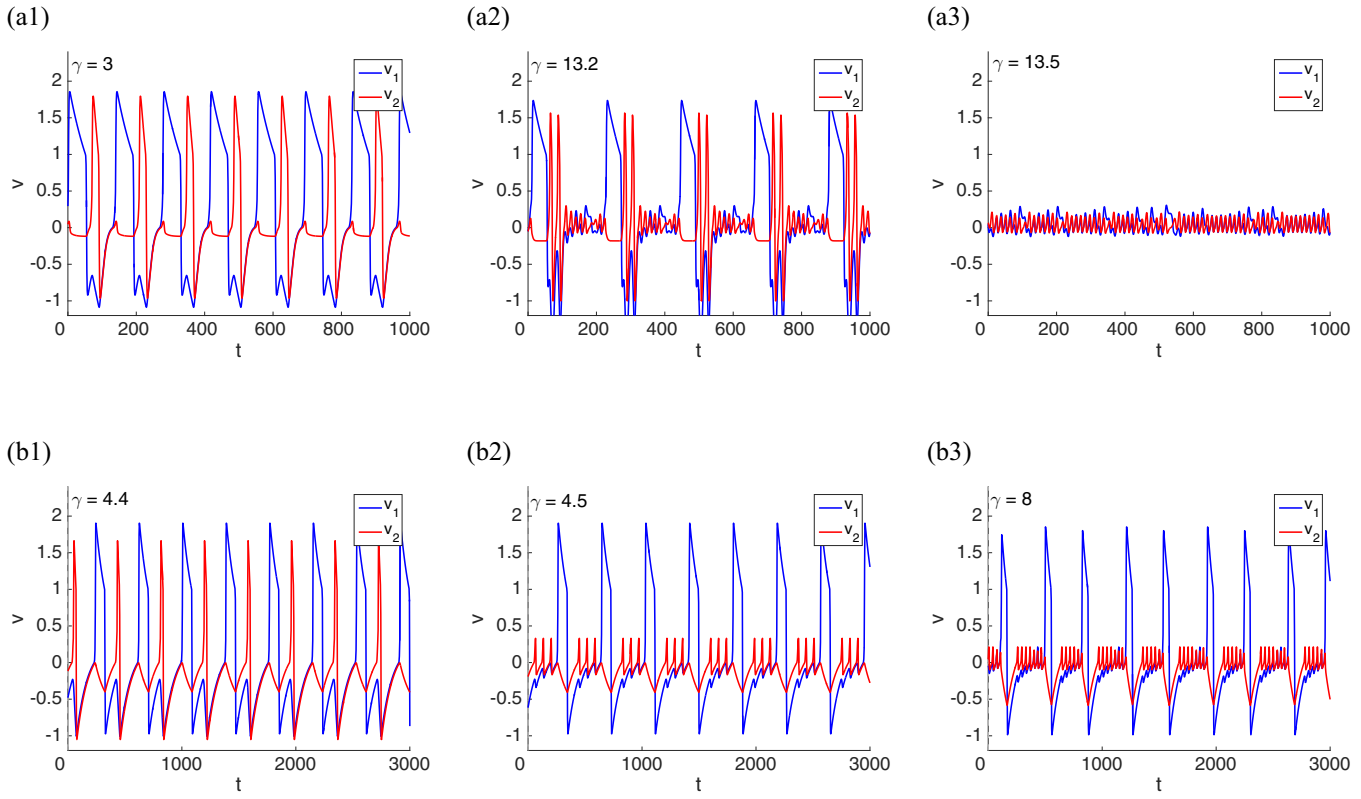

FIG. 9. Localized and nonlocalized patterns in a two-cluster network for representative values of γ. (a) Linearlike w-nullcline ($\beta_L = \beta_R = 1$). (b) Sigmoidlike w-nullcline ($\beta_L = \beta_R = 0.05$). We used the following parameter values: $\alpha = 2$, $\epsilon = 0.01$, $\lambda = 0.08$, $\sigma_1 = 0.2$, and $\sigma_2 = 0.8$,

of $\alpha = 4$). For the uncoupled system ($\gamma = 0$) and $\alpha = 2$, the PWL model fails to exhibit the canard phenomenon as λ changes. For the one-cluster system, in contrast, changes in γ are able induce the canard phenomenon, although for significantly larger values of γ_c than for $\alpha = 4$.

Our results in Figs. 9(b) show that for $\alpha = 2$ and sigmoidlike w-nullclines the abrupt transition between phase-locked and localized patterns has properties similar to those at $\alpha = 4$, but the abrupt transition occurs at much higher values of γ. In contrast, for linearlike w-nullclines the PWL model fails to produce localized patterns [Figs. 9(a)]. There is an abrupt transition from the LAO patterns in Fig. 9(a2) to the SAO patterns in Fig. 9(a3).

There are additional differences in the patterns in Figs. 9(a) versus Figs. 7(a) such as the occurrence of two LAOs per cycle at $\alpha = 2$ (not shown), which we did not observe at $\alpha = 4$.

I. Localized patterns are robust to changes in λ for the PWL model with a sigmoidlike w-nullcline but not for a linearlike w-nullcline

Increasing values of λ increase the global feedback critical value γ_c [Figs. 4(c)], and therefore it increases both $\gamma_{c,1}$ and $\gamma_{c,2}$ and is expected to increase the values of γ at which the transitions to localized patterns (if they exist) are present. If the values of γ are too high, then the v-nullcline flattens before the canard phenomenon can be induced by γ as for the case illustrated in Fig. 4(b3). Therefore, it is not clear *a priori* that the transitions shown at $\lambda = 0.08$ in Figs. 7 and 8 persist at larger values of λ. To address this issue we used the same parameter values as in these figures, but with $\lambda = 0.4$ (instead of $\lambda = 0.08$). Our results are presented in Fig. 10.

The model with a sigmoidlike w-nullcline [Figs. 10(b)] shows an abrupt transition from phase-locked LAOs to localized patterns with properties similar to those at $\lambda = 0.08$ [Figs. 7(b)]. In contrast, the patterns displayed for the model with a linearlike w-nullcline [Figs. 10(a)] differ from those at $\lambda = 0.08$. Importantly, for $\lambda = 0.4$ the model does not exhibit localized patterns. Other differences include the presence of in-phase patterns at low values of γ (e.g., $\gamma = 1$; not shown) and LAO localized patterns [Fig. 10(a2)] where the number of LAOs for O_2 per cycle increases with increasing values of γ (not shown). There is an abrupt transition between these patterns and the ones in Fig. 10(a3).

J. Localized patterns are more robust for the sigmoidlike w-nullcline than for the linearlike w-nullcline for larger values of ϵ

In Figs. 11(a) and 11(b) we show representative patterns for $\epsilon = 0.1$ and the parameter values from Figs. 4(a) and 4(b), respectively. In both cases, for low enough values of γ the system shows in-phase patterns [Figs. 11(a1) and 11(b1)], consistent with previous findings for the smooth FHN model [72].

As γ increases, the patterns in the PWL model with a linearlike w-nullcline transition to the complex type of patterns shown in Fig. 11(a2) and then to the synchronized in-phase

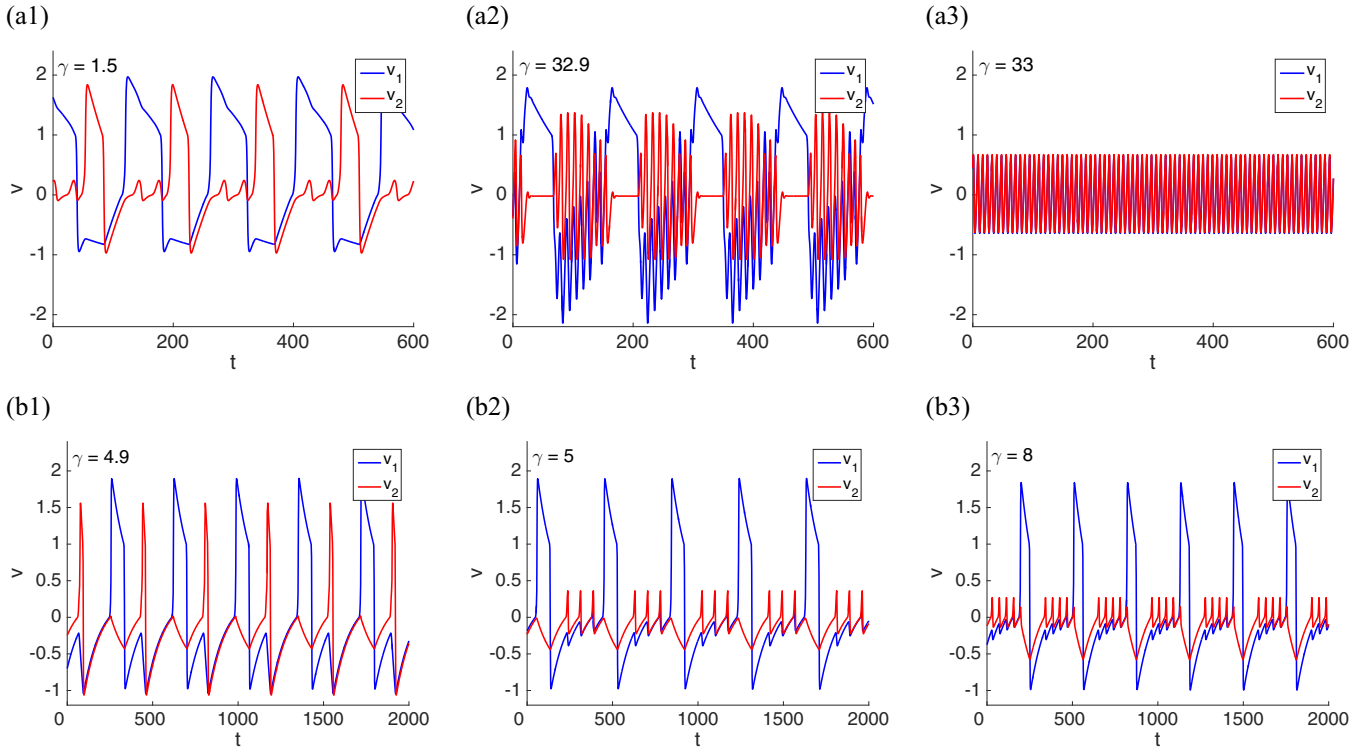

FIG. 10. Localized and nonlocalized patterns in a two-cluster network for representative values of γ. (a) Linearlike w-nullcline ($\beta_L = \beta_R = 1$). (b) Sigmoidlike w-nullcline ($\beta_L = \beta_R = 0.05$). We used the following parameter values: $\alpha = 4$, $\epsilon = 0.01$, $\lambda = 0.4$, $\sigma_1 = 0.2$, and $\sigma_2 = 0.8$.

patterns shown in Fig. 11(a3). The phase-plane diagrams for these patterns (not shown) are qualitatively similar to those obtained for the single-cluster case [Fig. 4(b1)], which does not exhibit the canard phenomenon as γ increases. The absence of localization for the two-cluster system is associated with this lack of ability of the single-cluster system to exhibit the γ-induced canard phenomenon.

In contrast, for the PWL model with a sigmoidlike w-nullcline (and the same value of λ) [Figs. 11(b)], as γ increases the patterns transition to the localized patterns shown in Figs. 11(b2) and 11(b3). The larger and smaller SAOs in Figs. 11(b2) and 11(b3) correspond to the limit-cycle trajectories crossing the linear pieces L_3 and L_2, respectively (not shown). A significant difference between these localized patterns and the ones for $\epsilon = 0.01$ [Figs. 7(b) and 10(b)] is that in the latter the SAOs are interrupted during LAOs, while in the former SAOs and LAOs may occur simultaneously.

While localization does not occur at $\lambda = 0.7$ in the PWL model with a linearlike w-nullcline, it may be restored at lower values of λ [Fig. 11(c3)]. For these parameter values the system also shows antiphase patterns [Fig. 11(b2)] at lower values of γ.

IV. DISCUSSION

Localized patterns in oscillatory networks where one oscillator (or cluster) exhibits LAOs or MMOs, while the other exhibits SAOs, have been observed both experimentally and theoretically [32–36,72,73,114–116]. In previous work we have established that these types of localized patterns can be obtained in networks of relaxation oscillators such as the FHN model and the Oregonator where the individual oscillators exhibit the supercritical canard phenomenon. In these networks, localized patterns required the presence of heterogeneity in the cluster distribution, which effectively creates heterogeneity in the intercluster connectivity. One important aspect of these networks is that the individual oscillators are monostable (they exhibit either LAOs or SAOs but not both). The symmetry break in the oscillation amplitude regime between the two (or more) clusters is a network phenomenon. However, how and under what conditions localized patterns emerge as the result of the interaction between the network connectivity and the intrinsic properties of the individual oscillators (e.g., the canard phenomenon) were not fully understood.

In this paper we set out to address these issues in the context of a PWL model of the FHN type where the v-nullcline is cubiclike and the w-nullcline is either sigmoid- or linearlike. This model belongs to the set of minimal models that are able to produce localized patterns. Oscillatory patterns in globally coupled models have also been studied using the so-called phase oscillators [37,75,117–122]. In these models, each oscillator is described solely by its phase and the effects of the interaction of oscillators on their amplitude is neglected by assuming weak coupling. These models are successful in capturing the phase-lock cluster patterns where the two oscillators are in the same amplitude regime, but they fail to capture the generation of more complex patterns that involve more than one oscillatory amplitude regime and transitions between both.

In order to identify the principles that govern how the interplay of the intrinsic properties of the individual oscillators and the network connectivity produces the localized patterns, we have considered a number of representative scenarios, which include qualitatively different types of w-nullclines

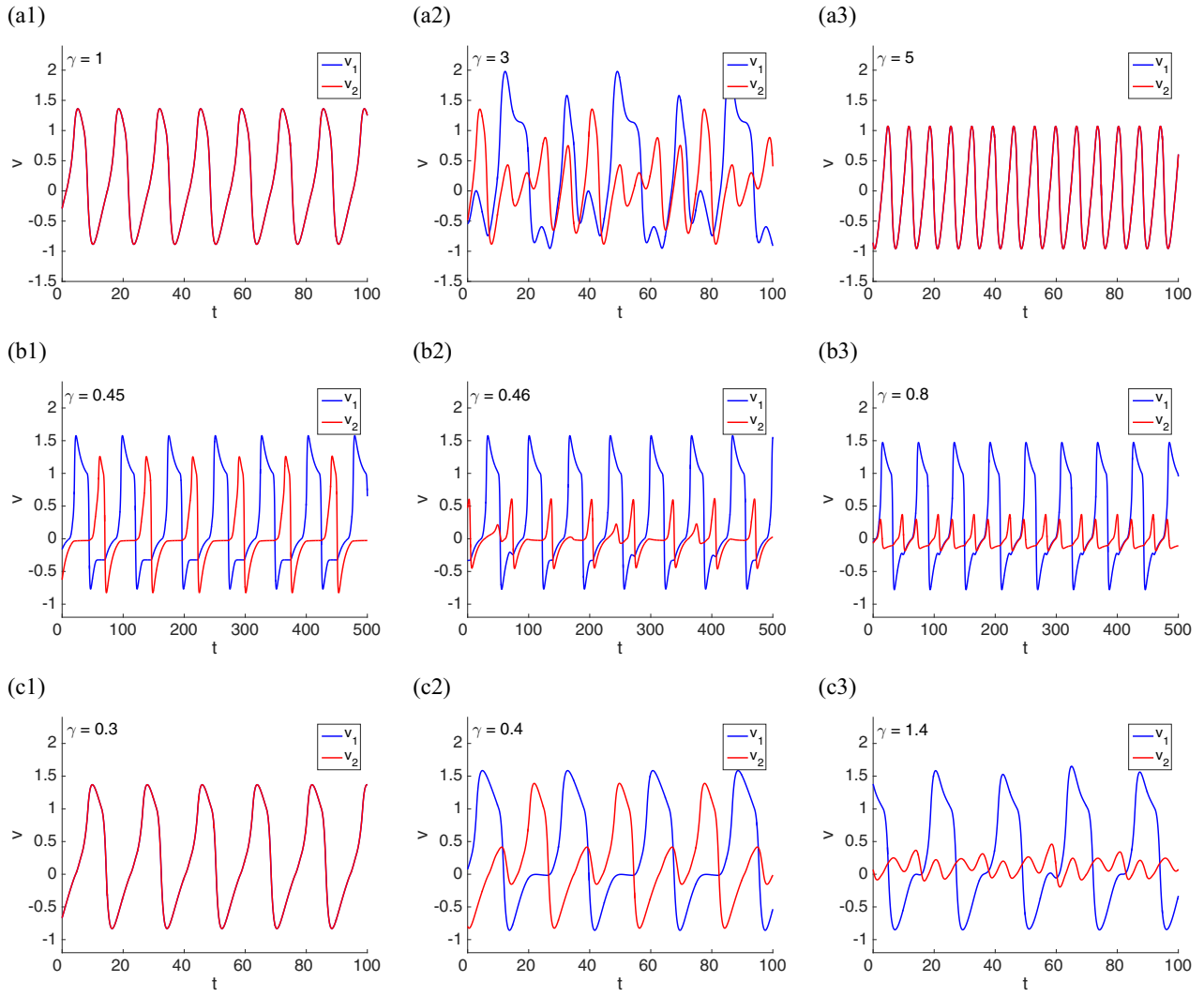

FIG. 11. Localization in a two-cluster network for representative values of γ. (a) Linearlike w-nullcline ($\beta_L = \beta_R = 1$) and $\lambda = 0.7$. (b) Sigmoidlike w-nullcline ($\beta_L = \beta_R = 0.05$) and $\lambda = 0.7$. **(c)** Linearlike w-nullcline ($\beta_L = \beta_R = 1$) and $\lambda = 0.4$. We used the following parameter values: $\alpha = 4$, $\epsilon = 0.1$, $\sigma_1 = 0.2$, and $\sigma_2 = 0.8$.

(sigmoid- and linearlike) and different parameter values that control the slope of the w-nullcline (α), its displacement with respect to the v-nullcline (λ), and the time-scale separation between the participating variables (ϵ).

Our results show that the presence of the supercritical canard phenomenon in the individual oscillatory clusters is a necessary ingredient to produce localized patterns, but it is not sufficient [e.g., Figs. 9(a) and 10(a)]. Localized patterns require a specific tuning between the various model parameters and the shape of the w-nullcline. In fact, the robustness of these patterns is strongly dependent on the shape of the w-nullcline. Models with a sigmoidlike w-nullcline produced more robust localized patterns than models with linearlike w-nullclines (e.g., Fig. 7) as well as abrupt transitions between phase-locked and localized patterns, which were absent in models with linearlike w-nullclines. The shape of the w-nullcline has additional effects on the network patterns. A salient one is the fact that the monotonic properties of the localized patterns' LAO frequency with changes in γ are different in models with sigmoidlike and linearlike w-nullclines. This is expected to have implications for realistic systems. However, the exact details of these implications remain to be understood.

The different types of cluster patterns we describe in this paper are stationary solutions in the corresponding larger networks, which result from using the cluster reduction of dimensions argument. Other stationary solutions are possible and the cluster solutions we found may not be stable. Our goal was to investigate under what conditions the localized (and other MMO) solutions are possible, what their properties are, how they depend on the interplay of the properties of the participating individual oscillators and the network connectivity, and what mechanisms govern the transition between the large-amplitude and the localized patterns. All this is necessary to understand how these types of patterns emerge in larger networks. Further research is needed to clarify these points, to examine how cluster patterns arise in these larger networks from "noncluster" initial conditions, and what their stability properties are [123].

In this paper we have considered a specific type of global coupling motivated by previous work. Other studies

have considered global feedback from the activator variable onto itself, rather than from the inhibitor onto the activator [69,124–127]. More research is needed to establish whether and under what conditions localized patterns are possible in these networks and, if they exist, to characterize the similarities and differences between the patterns generated by the two types of global feedback.

An alternative scenario to the one we present here involves the presence of bistability in the individual oscillators [108]. In this case, the role of the network connectivity is to separate the oscillators into clusters by causing each oscillator to choose between the stationary solutions of the individual oscillators. This will require the presence of bistability between two oscillatory regimes. Alternatively, the localized solutions would involve one oscillatory and one silent cluster.

An additional goal of this study was to explore the effects of the interplay between the two competing types of coupling: global inhibition and diffusion (see Appendix B). Global inhibition tends to create clusters. Diffusion is local and tends to cause oscillators to synchronized in-phase. Indeed, when the two clusters are of equal size and the oscillators are initially in the LAO regime, the addition of diffusion causes them to synchronize in-phase either in the LAO or in the SAO regime, depending on the D_v/γ ratio. However, when the cluster sizes are different, the addition of diffusion induced localized or MMO network patterns that were either synchronized in-phase or not, depending also on the D_v/γ ratio. Even when the resulting patterns are synchronized in-phase, they do not resemble the patterns in the absence of diffusion.

We emphasize that the diffusive type of coupling we used in this paper is not realistic and does not reflect the diffusive effects between oscillators in each cluster in the original system. The questions of how oscillators in each cluster are held together and how the different cluster sizes are generated as the result of the interplay of global coupling and diffusion remain open.

Network patterns can be generated by various mechanisms. On one extreme, these patterns can be imposed by the network connectivity, with little or no participation of the individual oscillators. Our results highlight the richness of the patterns generated by the interplay of the network connectivity and the intrinsic properties of the individual oscillators.

ACKNOWLEDGMENT

This work was partially supported by National Science Foundation Grant No. DMS-1313861 (H.G.R.).

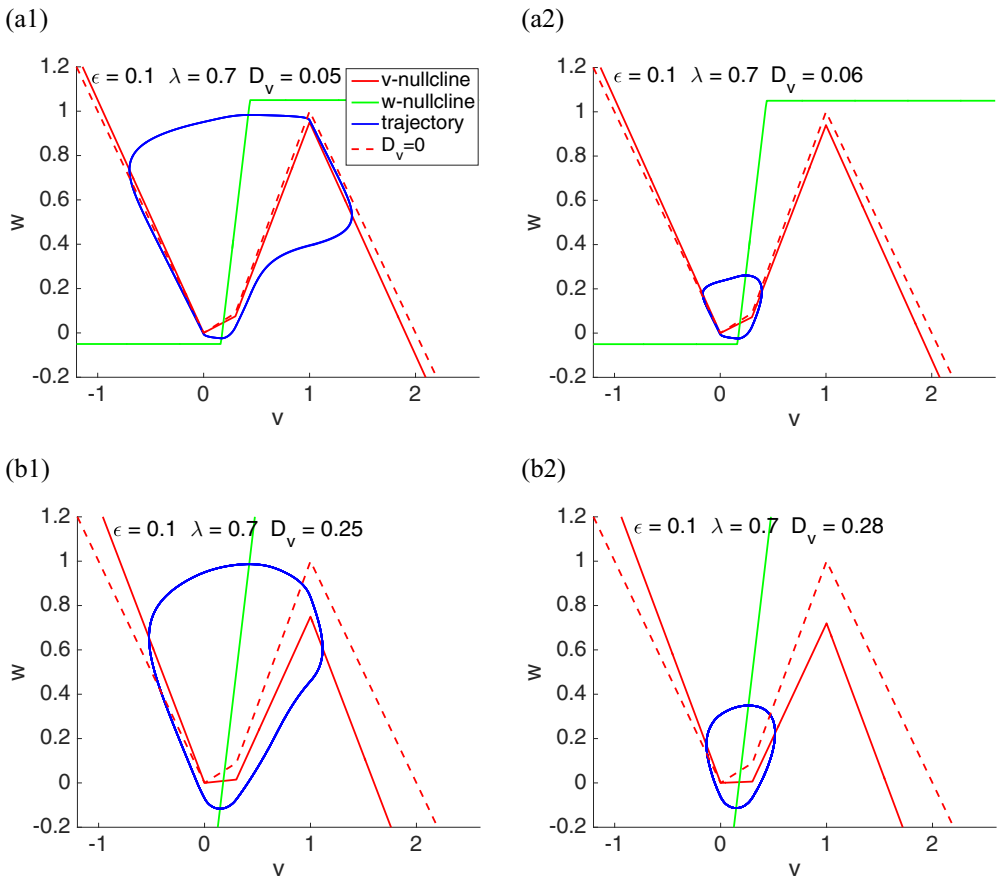

FIG. 12. Canard phenomenon induced by diffusion in bulk oscillatory systems. Parameter values are as in Fig. 4. The baseline v-nullcline for $\gamma = 0$ (dashed red line) is as in Fig. 1 and is presented for reference. The solid red v-nullcline corresponds to the actual values of γ used in each panel. For the w-nullcline we used the following parameter values: (a) $\alpha = 4$, $\epsilon = 0.1$, $\lambda = 0.7$, $\beta_L = -0.05$, and $\beta_R = 0.05$; (b) $\alpha = 4$, $\epsilon = 0.1$, $\lambda = 0.7$, $\beta_L = -1$, and $\beta_R = 1$; and (c) $\alpha = 4$, $\epsilon = 0.01$, $\lambda = 0.08$, $\beta_L = -1$, and $\beta_R = 1$.

APPENDIX A: DYNAMICS OF THE LINEAR REGIME

The dynamics of Eqs. (1)–(3) in each linear regime are governed by a system of the form

$$\begin{aligned} v' &= \eta\, v - w, \\ w' &= \epsilon\, [\, \alpha\, v - w\,], \end{aligned} \tag{A1}$$

where the fixed point $(\bar{v},\bar{w})$ (virtual or actual) has been translated to the origin and η represents the slope of the corresponding linear piece. The coordinates of the fixed point $(\bar{v},\bar{w})$ for each regime are given by

$$\bar{v} = \frac{\kappa\,\lambda - \eta\,\hat{v} + \hat{w}}{\kappa\,\alpha - \eta} \quad \text{and} \quad \bar{w} = \kappa\,\frac{\lambda\,\eta - \alpha\,\eta\,\hat{v} + \alpha\,\hat{w}}{\kappa\,\alpha - \eta}, \tag{A2}$$

where $f(v)$ is described by $\eta\,(v - \hat{v}) + \hat{w}$. Note that here we are using the same notation for the translated system, (A1), and the original system.

The case $\kappa = 1$ corresponds to the uncoupled system, while the case $\kappa = 1 + \sigma\,\gamma$ corresponds to the autonomous part of the globally coupled system, (7). The effects of D_v are included in the parameter η.

The eigenvalues for each fixed point are given by

$$r_{1,2} = \frac{\eta - \epsilon \pm \sqrt{(\eta+\epsilon)^2 - 4\,\kappa\,\epsilon\,\alpha}}{2}. \tag{A3}$$

The fixed points for the linear regime, (A1), are stable if $\eta < \epsilon$ and unstable if $\eta > \epsilon$. They are foci if

$$|\,\eta + \epsilon\,| < 2\sqrt{\kappa\,\epsilon\,\alpha} \tag{A4}$$

and nodes otherwise. Since $\alpha \geqslant 0$ and $\kappa > 0$, saddles are possible only for $\alpha = 0$. We refer the reader to [77] for a more detailed discussion for the case $\kappa = 1$. The global feedback parameter $\gamma > 0$ affects both the location of the fixed points and the eigenvalues. For large enough values of γ a node can transition into a focus.

APPENDIX B: INTERPLAY OF DIFFUSION (LOCAL) AND GLOBAL COUPLING

1. The canard phenomenon can be induced by the diffusion autonomous component

Global feedback and diffusion have opposite effects. While global feedback favors the generation of phase-locked clusters (Fig. 6), diffusion favors in-phase synchronization [Fig. 13(a)]. In the next sections we investigate the combined effect of global coupling and diffusion. Here, we look at the effects of the diffusion coefficient D_v on the dynamics of the autonomous part of system (10). This is not a realistic situation, but, as for the effects of γ on the one-cluster systems discussed in Sec. III B, it provides information on the dynamics of the autonomous part of each oscillator.

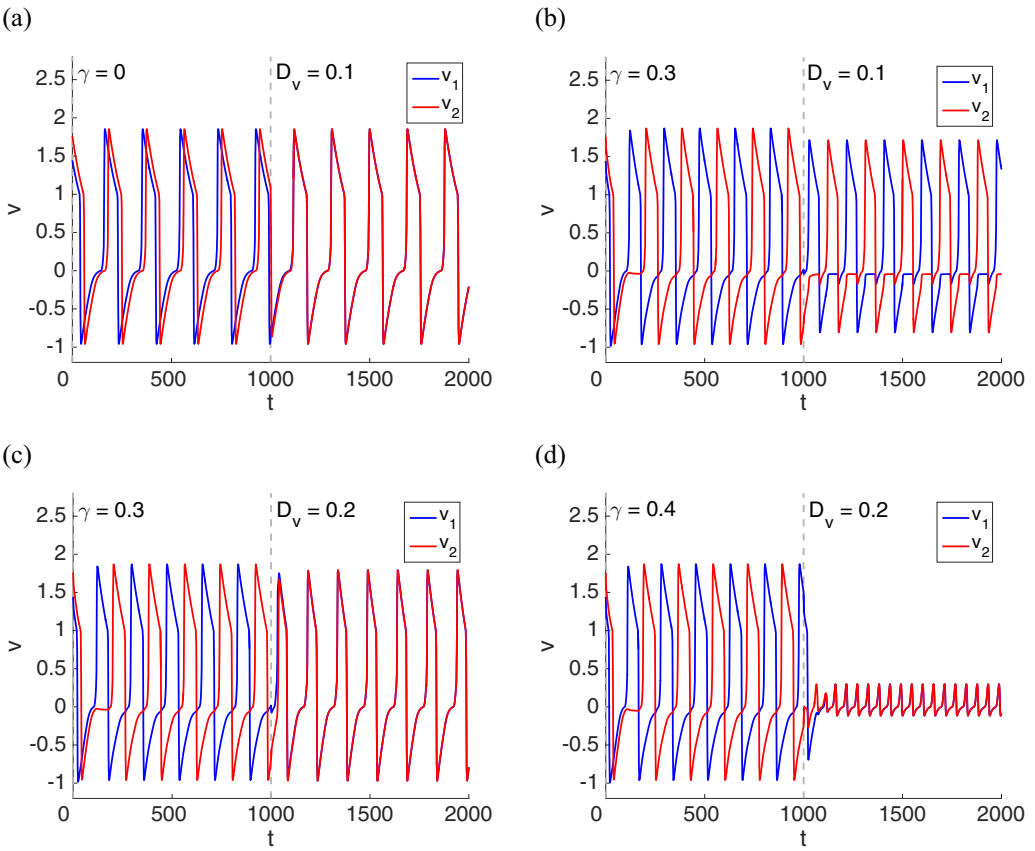

FIG. 13. Interplay of global coupling and diffusion in a two-cluster network for representative values of γ. We used the following parameter values: $\alpha = 4$, $\epsilon = 0.01$, $\lambda = 0.08$, $\sigma_1 = 0.5$, $\sigma_2 = 0.5$, $\beta_L = \beta_R = 0.05$. The dashed gray line indicates the time at which diffusion was activated.

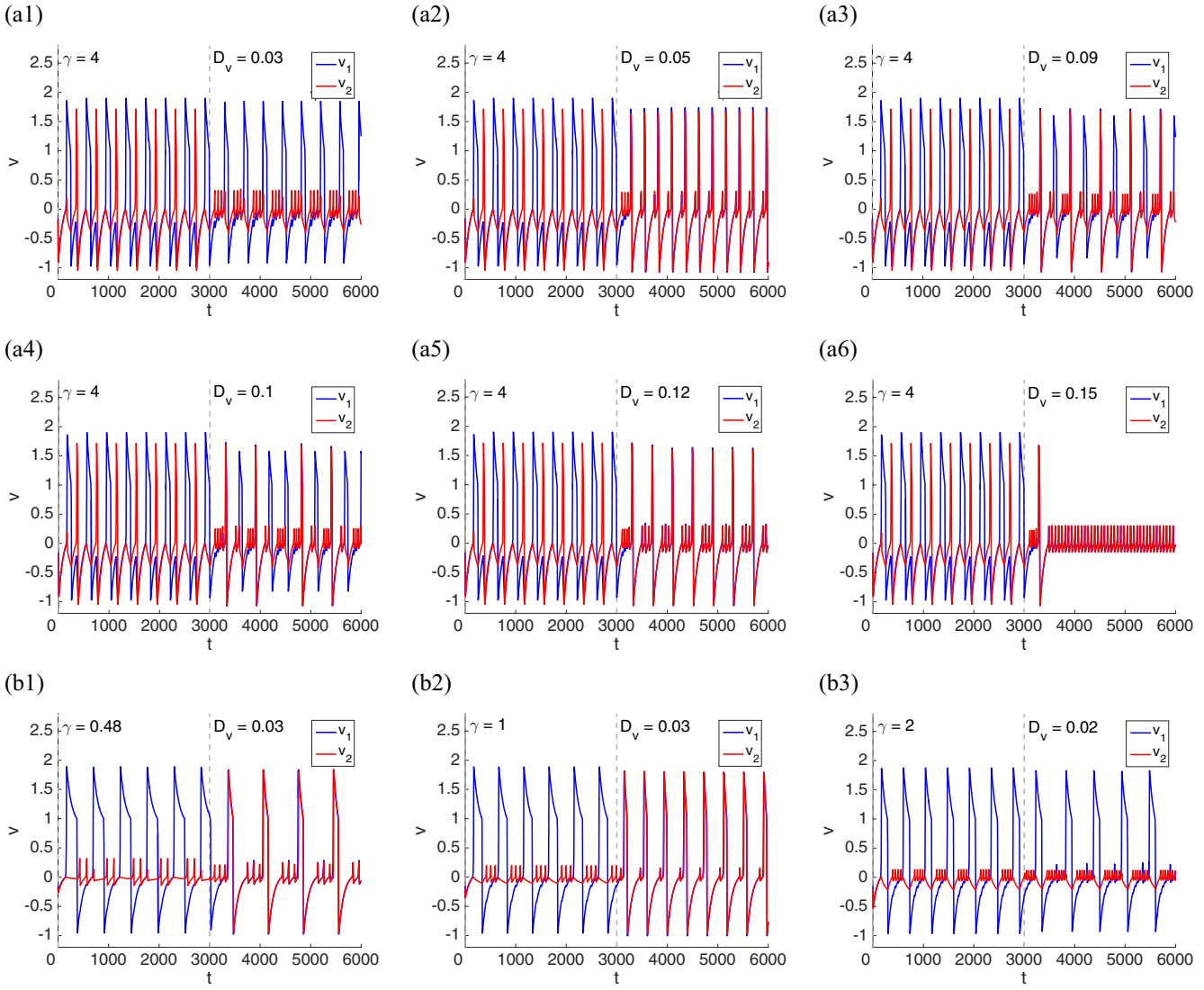

FIG. 14. Interplay of global coupling and diffusion in a two-cluster network for representative values of γ and a sigmoidlike w-nullcline. (a) $\lambda = 0.4$; (b) $\lambda = 0.08$. We used the following parameter values: $\alpha = 4$, $\epsilon = 0.01$, $\sigma_1 = 0.2$, $\sigma_2 = 0.8$, and $\beta_L = \beta_R = 0.05$. The dashed gray line indicates the time at which diffusion was activated.

Increasing values of D_v decrease the slopes (η) of the linear pieces L_2 and L_3. From (A4) this can cause the transition of the actual fixed point in R_2 from a node to a focus, therefore favoring the occurrence of the canard phenomenon. This is illustrated in Fig. 12 for the same parameter values as in Fig. 4 and $\gamma = 0$. [The baseline v-nullclines for $D_v = 0$ in Figs. 12(a), 12(b) and 12(c) are as in Figs. 4(a1), 4(b1), and 4(c1), respectively.]

2. Interplay of diffusion and global feedback for equal-size clusters: In-phase synchronization and the canard phenomenon

Here and in the next section we investigate the patterns that result from the interplay of global coupling and diffusion. For visualization purposes, in Figs. 13 and 14 we present the patterns for the globally coupled system in the absence of diffusion to the left of the dashed gray line. In a separate set of simulations we have checked that the patterns for both $\gamma > 0$ and $D_v > 0$ (right of the dashed gray line) remain unchanged when global feedback and diffusion are activated simultaneously (not shown).

For relatively low D_v/γ ratios, the system shows antiphase patterns (Fig. 13). As this ratio increases, the two oscillators synchronize in-phase [Fig. 13(c)]. In-phase patterns are also obtained for $\gamma = 0.3$ and $D_v = 0.15$ (not shown), for which $D_v/\gamma = 0.5$. For larger values of γ but similar D_v/γ ratios, the two oscillators exhibit in-phase SAOs. The increase in D_v does not always cause the transition from LAOs to SAOs since once the two oscillators synchronize in-phase they behave as a single cluster and the diffusive effects are negligible. Therefore, the transition from LAOs to SAOs in these cases depends on whether or not $\gamma > \gamma_c$. For example, for $\gamma = 0.3$ and values of D_v larger than the one in Fig. 13(c) the patterns remain in the LAO regime, in contrast to the patterns in Fig. 13(d).

3. Interplay of diffusion and global feedback for clusters of different sizes: Diffusion-induced localized and MMO patterns

In Fig. 14(a1) we illustrate the diffusion-induced localized patterns for the same parameter values as in Figs. 10(b) and a relatively low D_v/γ ratio. In the absence of diffusion, the system exhibits phase-locked LAOs and localization is induced by increasing values of γ [Figs. 10(b)]. Similar patterns were obtained for other values of γ and low D_v/γ ratios.

As D_v increases, different types of MMO patterns emerge [Figs. 14(a2) to 14(a5)], which combine the two competing effects of global coupling and diffusion. These patterns include in-phase MMO patterns with different ratios of SAOs and LAOs per cycle [e.g., Figs. 14(a2) and 14(a5)] and MMO patterns where the LAOs in both oscillators are phase-locked [e.g., Figs. 14(a3) and 14(a4)]. As D_v increases further, the system exhibits in-phase SAOs.

In Figs. 14(b) we show some representative patterns for low D_v/γ ratios. Figure 14(b1) shows a transition from localized to in-phase MMO patterns [similar to that in Fig. 14(a5)] that combine the features of both oscillators when $D_v = 0$. The in-phase MMOs have a lower LAO frequency than the localized pattern for $D_v = 0$. Figure 14(b2) also shows a transition between localized and in-phase MMOs. However, these MMOs have fewer SAOs per cycle and a higher LAO frequency than for $D_v = 0$. Finally, in Fig. 14(b3) there is a transition between two types of localized patterns with different ratios of SAOs per cycle and a lower frequency. In all cases, there is a relatively abrupt transition between these patterns and SAO patterns, often not synchronized in-phase (not shown). These transitions sometimes involve irregular patterns for very small ranges of D_v.

[1] S. H. Strogatz, *Nonlinear Dynamics and Chaos* (Addison Wesley, Reading MA, 1994).

[2] F. Sagués and I. R. Epstein, Nonlinear chemical dynamics, Dalton Trans. **2003**, 1201 (2003); https://www.deepdyve.com/lp/royal-society-of-chemistry/nonlinear-chemical-dynamics-eVRizocmgA.

[3] J. D. Murray, *Mathematical Biology: I. An Introduction* (Springer, Berlin, 2002).

[4] J. Keener and J. Sneyd, *Mathematical Physiology* (Springer-Verlag, New York, 2001).

[5] G. B. Ermentrout and D. Terman, *Mathematical Foundations of Neuroscience* (Springer, Berlin, 2010).

[6] A. T. Winfree, *The Geometry of Biological Time*, 2nd ed. (Springer-Verlag, New York, 2001).

[7] I. R. Epstein and J. A. Pojman, *An Introduction to Nonlinear Chemical Dynamics* (Oxford University Press, New York, 1998).

[8] B. P. Belousov, A periodic reaction and its mechanism, Compil. Abstr. Radiat. Med. (Med. Publ., Moscow) **147**, 145 (1959).

[9] A. M. Zhabotinsky, Periodic processes of malonic acid oxidation in a liquid phase, Biofizika **9**, 306 (1964).

[10] A. Goldbeter, *Biochemical Oscillations and Cellular Rhythms: The Molecular Basis of Periodic and Chaotic Behavior* (Cambridge University Press, Cambridge, UK, 1996).

[11] B. van der Pol, On relaxaction oscillations I, Philos. Mag. **2**, 978 (1926).

[12] R. FitzHugh, Thresholds and plateaus in the Hodgkin-Huxley nerve equations, J. Gen. Physiol. **43**, 867 (1960).

[13] J. S. Nagumo, S. Arimoto, and S. Yoshizawa, An active pulse transmission line simulating nerve axon, Proc. IRE **50**, 2061 (1962).

[14] R. J. Fields and R. M. Noyes, Oscillations in chemical systems. IV. Limit cycle behavior in a model of a real chemical oscillation, J. Chem. Phys. **60**, 1877 (1974).

[15] B. P. Belousov, A periodic reaction and its mechanism, in *Oscillations and Traveling Waves in Chemical Systems*, edited by R. J. Field and M. Burger (Wiley, New York, 1985), pp. 605–613.

[16] A. M. Zhabotinsky, F. Buchholtz, A. B. Kiyatkin, and I. R. Epstein, Oscillations and waves in metal-ion-catalyzed bromate oscillating reactions in highly oxidized states, J. Phys. Chem. **97**, 7578 (1993).

[17] H. Morris and C. Lecar, Voltage oscillations in the barnacle giant muscle fiber, Biophys. J. **35**, 193 (1981).

[18] L. Segel and A. Goldbeter, Scaling in biochemical kinetics: Dissection of a relaxation oscillator, J. Math. Biol. **32**, 147 (1994).

[19] A. Goldbeter and R. Lefever, Dissipative structures for an allosteric model: Application to glycolytic oscillations, Biophys. J. **12**, 1302 (1972).

[20] D. Gonze, N. Markadieu, and A. Goldbeter, Selection of in-phase or out-of-phase synchronization in a model based on global coupling of cells undergoing metabolic oscillations, Chaos **18**, 037127 (2008).

[21] P. Westermark and A. Lansner, A model of the phosphofructokinase and glycolytic oscillations in pancreating β-cell, Biophys. J. **85**, 126 (2003).

[22] R. Guantes and J. Poyatos, Dynamical principles of two-component genetic oscillators, PLoS Comput. Biol. **2**, e30 (2006).

[23] F. Dumortier and R. Roussarie, Canard cycles and center manifolds, Mem. Am. Math. Soc. **121**, 577 (1996).

[24] W. Eckhaus, Relaxation oscillations including a standard chase on French ducks, in *Lecture Notes in Mathematics* (Springer-Verlag, Berlin, 1983), Vol. 985, pp. 449–497.

[25] S. M. Baer and T. Erneux, Singular Hopf bifurcation to relaxation oscillations, SIAM J. Appl. Math. **52**, 1651 (1992).

[26] E. Benoit, J. L. Callot, F. Diener, and M. Diener, Chasse au canard, Collect. Math. **31–32**, 37 (1981).

[27] M. Krupa and P. Szmolyan, Relaxation oscillation and canard explosion, J. Diff. Eqs. **174**, 312 (2001).

[28] M. Krupa and P. Szmolyan, Extending geometric singular perturbation theory to nonhyperbolic points—Fold and canard points in two dimensions, SIAM J. Math. Anal. **33**, 286 (2001).

[29] F. Dumortier, Techniques in the theory of local bifurcations: Blow-up, normal forms, nilpotent bifurcations, singular perturbations, in *Bifurcations and Periodic Orbits of Vector Fields*, edited by D. Schlomiuk (Kluwer Academic Press, Dordrecht, Netherlands, 1993), pp. 19–73.

[30] M. Brøns, T. J. Kaper, and H. G. Rotstein, Introduction to focus issue: Mixed mode oscillations: Experiment, computation, and analysis, Chaos **18**, 015101 (2008).
[31] M. Desroches, J. Guckenheimer, B. Krauskopf, C. Kuehn, H. M. Osinga, and M. Wechselberger, Mixed-mode oscillations with multiple time scales, SIAM Rev. **54**, 211 (2012).
[32] V. K. Vanag, L. Yang, M. Dolnik, A. M. Zhabotinsky, and I. R. Epstein, Oscillatory cluster patterns in a homogeneous chemical system with global feedback, Nature **406**, 389 (2000).
[33] V. K. Vanag, A. M. Zhabotinsky, and I. R. Epstein, Pattern formation in the Belusov-Zhabotinsky reaction with photochemical global feedback, J. Phys. Chem. A **104**, 11566 (2000).
[34] L. Yang, M. Dolnik, A. M. Zhabotinsky, and I. R. Epstein, Oscillatory clusters in a model of the photosensitive Belusov-Zhabotinsky reaction system with global feedback, Phys. Rev. E **62**, 6414 (2000).
[35] H. G. Rotstein, N. Kopell, A. Zhabotinsky, and I. R. Epstein, A canard mechanism for localization in systems of globally coupled oscillators, SIAM J. Appl. Math. **63**, 1998 (2003).
[36] H. G. Rotstein, N. Kopell, A. Zhabotinsky, and I. R. Epstein, Canard phenomenon and localization of oscillations in the Belousov-Zhabotinsky reaction with global feedback, J. Chem. Phys. **119**, 8824 (2003).
[37] A. F. Taylor, P. Kapetanopoulos, B. J. Whitaker, R. Toth, L. Bull, and M. R. Tinsley, Phase clustering in globally coupled photochemical oscillators, Eur. Phys. J.: Spec. Top. **165**, 137 (2008).
[38] M. Bertram, C. Beta, M. Pollmann, A. S. Mikhailov, H. H. Rotermund, and G. Ertl, Pattern formation on the edge of chaos: Experiments with CO oxidation on a Pt(110) surface under global delayed feedback, Phys. Rev. E **67**, 036208 (2003).
[39] M. Bertram and A. S. Mikhailov, Pattern formation on the edge of chaos: Mathematical modeling of CO oxidation on a Pt(110) surface under global delayed feedback, Phys. Rev. E **67**, 036207 (2003).
[40] M. Kim, M. Bertram, M. Pollmann, A. von Oertzen, A. S. Mikhailov, H. H. Rotermund, and G. Ertl, Controlling chemical turbulence by global delayed feedback: Pattern formation in catalytic CO oxidation on Pt(110), Science **292**, 1357 (2001).
[41] F. Plenge, P. Rodin, E. Schöll, and K. Krischer, Breathing current domains in globally coupled electrochemical systems: A comparison with a semiconductor model, Phys. Rev. E **64**, 056229 (2001).
[42] F. Plenge, Y.-J. Li, and K. Krischer, Spatial bifurcations in the generic N-NDR electrochemical oscillator with negative global coupling: Theory and surface plasmon experiments, J. Phys. Chem. B **108**, 14255 (2004).
[43] N. Baba and K. Krischer, Mixed-mode oscillations and cluster patterns in an electrochemical relaxation oscillator under galvanostatic control, Chaos **18**, 015103 (2008).
[44] W. Wang, I. Z. Kiss, and J. L. Hudson, Experiments on arrays of globally coupled chaotic electrochemical oscillators: Synchronization and clustering, Chaos **10**, 248 (2000).
[45] I. Z. Kiss, W. Wang, and J. L. Hudson, Populations of coupled electrochemical oscillators, Chaos **12**, 252 (2002).
[46] I. Z. Kiss, Y. Zhai, and J. L. Hudson, Resonance Clustering in Globally Coupled Electrochemical Oscillators with External Forcing, Phys. Rev. E **77**, 046204 (2008).
[47] V. García-Morales, A. Orlov, and K. Krischer, Subharmonic phase clusters in the complex Ginzburg-Landau equation with nonlinear global coupling, Phys. Rev. E **82**, 065202 (2010).
[48] V. García Morales and K. Krischer, Normal-form approach to spatiotemporal pattern formation in globally coupled electrochemical systems, Phys. Rev. E **78**, 057201 (2008).
[49] S. Yu. Kourtchatov, V. V. Likhanskii, A. P. Napartovich, F. T. Arecchi, and A. Lapucci, Theory of phase locking of globally coupled laser arrays, Phys. Rev. A **52**, 4089 (1995).
[50] M. A. Liauw, P. J. Plath, and N. I. Jaeger, Complex oscillations and global coupling during the catalytic oxidation of CO, J. Chem. Phys. **104**, 6375 (1996).
[51] K. Miyakawa and K. Yamada, Synchronization and clustering in globally coupled salt-water oscillators, Physica D **151**, 217 (2001).
[52] Y. X. Li, J. Halloy, J. L. Martiel, and A. Goldbeter, Suppression of chaos and other dynamical transitions induced by intercellular coupling in a model of cyclic AMP signaling in Dictyostelium cells, Chaos **2**, 501 (1992).
[53] A. Khadra and Y. X. Li, A model for the pulsatile secretion of gonadotropin-releasing hormone from synchronized hypothalamic neurons, Biophys. J. **91**, 74 (2006).
[54] E. Alvarez-Lacalle, J. F. Rodriguez, and B. Echebarria, Oscillatory regime in excitatory media with global coupling: Application to cardiac dynamics, Comput. Cardiol. **35**, 189 (2008).
[55] E. Alvarez-Lacalle and B. Echebarria, Global coupling in excitable media provides a simplified description of mechano-electrical feedback in cardiac tissue, Phys. Rev. E **79**, 031921 (2009).
[56] A. F. Taylor, M. R. Tinsley, F. Wang, Z. Huang, and K. Showalter, Dynanical quorum sensing and synchronization in large populations of chemical oscillators, Science **323**, 614 (2009).
[57] S. De Monte, F. d'Ovidio, S. Danø, and P. G. Sørensen, Dynamical quorum sensing: Population density encoded in cellular dynamics, Proc. Natl. Acad. Sci. USA **104**, 18377 (2007).
[58] J. Wolf and R. Heinrich, Dynamics of two-component biochemical systems in interacting cells; Synchronization and desynchronization of oscillations and multiple steady states, BioSystems **43**, 1 (1997).
[59] J. Wolf, J. Passarge, O. J. Somsen, J. L. Snoep, R. Heinrich, and H. V. Westerhoff, Transduction of intracellular and intercellular dynamics in yeast glycolytic oscillation, Biophys. J. **78**, 1145 (2000).
[60] J. García-Ojalvo, S. H. Elowitz, and M. B. Strogatz, Modeling a synthetic multicellular clock: Repressilators coupled by quorum sensing, Proc. Natl. Acad. Sci. USA **101**, 10955 (2004).
[61] C. Liu, D. R. Weaver, S. H. Strogatz, and S. M. Reppert, Cellular construction of a circadian clock: Period determination in the suprachiasmatic nuclei, Cell **91**, 855 (1997).
[62] D. Gonze, S. Bernard, C. Waltermann, A. Kramer, and H. Herzel, Spontaneous synchronization of coupled circadian oscillators, Biophys. J. **89**, 120 (2005).
[63] L. To, M. A. Henson, E. D. Herzog, and F. J. Doyle III, A molecular model for intercellular synchronization in the mammalian circadian clock, Biophys. J. **92**, 3792 (2007).
[64] D. Golomb and J. Rinzel, Clustering in globally coupled inhibitory neurons, Physica D **72**, 259 (1994).

[65] D. Terman and D. L. Wang, Global competition and local cooperation in a network of neural oscillators, Physica D **81**, 148 (1995).
[66] J. Rubin and D. Terman, Analysis of clustered firing patterns in synaptically coupled networks of oscillators, J. Math. Biol. **41**, 513 (2000).
[67] D. M. Durand, E.-H. Park, and A. L. Jensen, Potassium diffusive coupling in neural networks, Philos. Trans. R. Soc. London B **365**, 2347 (2010).
[68] M. G. Rosenblum and A. S. Pikovsky, Controlling Synchronization in an Ensemble of Globally Coupled Oscillators, Phys. Rev. Lett. **92**, 114102 (2004).
[69] R. A. Stefanescu and V. K. Jirsa, A low dimensional description of globally coupled heterogeneous neural networks of excitatory and inhibitory neurons, PLoS Comput. Biol. **4**, e1000219 (2008).
[70] D. Wang, Relaxation oscillators and networks, in *Encyclopedia of Electrical and Electronics Engineering*, Vol. 18, edited by J. G. Webster (Wiley & Sons, 1999), pp. 396–405.
[71] M. Bertram and A. S. Mikhailov, Pattern formation in a surface chemical reaction with global delayed feedback, Phys. Rev. E **63**, 066102 (2001).
[72] H. G. Rotstein and H. Wu, Swing, release, and escape mechanisms contribute to the generation of phase-locked cluster paterns in a globally coupled Fitzhugh-Nagumo model, Phys. Rev. E **86**, 066207 (2012).
[73] H. G. Rotstein and H. Wu, Dynamic mechanisms of generation of oscillatory cluster patterns in a globally coupled chemical system, J. Chem. Phys. **137**, 104908 (2012).
[74] D. Golomb, X.-J. Wang, and J. Rinzel, Synchronization properties of spindle oscillations in a thalamic reticular nucleus model, J. Neurophysiol. **72**, 1109 (1994).
[75] D. Golomb, D. Hansel, B. Shraiman, and H. Sompolinksy, Clustering in globally coupled phase oscillators, Phys. Rev. A **45**, 3516 (1992).
[76] H. G. Rotstein, T. Oppermann, J. A. White, and N. Kopell, A reduced model for medial entorhinal cortex stellate cells: Subthreshold oscillations, spiking and synchronization, J. Comput. Neurosci. **21**, 271 (2006).
[77] H. G. Rotstein, S. Coombes, and A. M. Gheorghe, Canard-like explosion of limit cycles in two-dimensional piecewise-linear models of FitzHugh-Nagumo type, SIAM J. Appl. Dynam. Syst. **11**, 135 (2012).
[78] H. P. McKean, Nagumo's equation, Adv. Math. **4**, 209 (1970).
[79] W. P. Wang, Multiple impulse solutions to McKean's caricature of the nerve equation. I. Existence, Commun. Pure Appl. Math. **41**, 71 (1988).
[80] W. P. Wang, Multiple impulse solutions to McKean's caricature of the nerve equation. II. Stability, Commun. Pure Appl. Math. **41**, 997 (1988).
[81] A. Tonnelier, The McKean's caricature of the FitzHugh-Nagumo model. I. The space-clamped system, SIAM J Appl. Math. **63**, 459 (2002).
[82] J. Rinzel and J. B. Keller, Traveling wave solutions of a nerve conduction equation, Biophys. J. **13**, 1313 (1973).
[83] J. Rinzel, Neutrally stable traveling wave solutions of nerve conduction equations, J. Math. Biol. **2**, 205 (1975).
[84] J. Rinzel, Spatial stability of traveling wave solutions of a nerve conduction equation, Biophys. J. **15**, 975 (1975).
[85] S. Coombes and A. H. Osbaldestin, Period adding bifurcations and chaos in a periodically stimulated excitable neural relaxation oscillator, Phys. Rev. E **62**, 4057 (2000).
[86] A. Tonnelier and W. Gerstner, Piecewise linear differential equations and integrate-and-fire neurons: Insights from two-dimensional membrane models, Phys. Rev. E **67**, 021908 (2003).
[87] S. Coombes, Neuronal networks with gap junctions: A study of piece-wise linear planar neuron models, SIAM J. Appl. Dynam. Syst. **7**, 1101 (2008).
[88] S. J. Hogan, On the dynamics of rigid-block motion under harmonic forcing, Proc. R. Soc. London A **425**, 441 (1989).
[89] S. H. Doole and S. J. Hogan, Non-linear dynamics of the extended Lazer-McKenna bridge oscillation model, Dynam. Stabil. Syst. **15**, 43 (2000).
[90] M. di Bernardo, C. Budd, A. R. Champneys, and P. Kowalczyk, *Piecewise-Smooth Dynamical Systems: Theory and Applications* (Springer, Berlin, 2007).
[91] G. M. Maggio, M. di Bernardo, and M. P. Kennedy, Nonsmooth bifurcations in a piecewise-linear model of the Colpitts oscillator, IEEE Trans. Circuits Syst. I **47**, 1160 (2000).
[92] A. F. Filippov, *Differential Equations with Discontinuous Righthand Sides* (Kluwer Academic, Dordrecht, Netherlands, 1988).
[93] E. Plahte and S. Kjoglum, Analysis and generic properties of gene regulatory networks with graded response functions, Physica D **201**, 150 (2005).
[94] F. Grognard, H. de Jong, and J.-L. Gouzé, *Biology and Control Theory: Current Challenges*. *Lecture Notes in Control and Information Science (LNCIS) 357*, edited by I. Queinnec, S. Tarbouriech, G. Garcia, and S. Niculescu (Springer, Berlin, 2007).
[95] J. Llibre, E. Nuñez, and A. E. Teruel, Limit cycles for planar piecewise linear differential systems via first integrals, Qual. Theory Dynam. Syst. **3**, 29 (2002).
[96] E. Freire, E. Ponce, F. Rodrigo, and F. Torres, Bifurcation sets of continuous piecewise linear systems with two zones, Int. J. Bifurcat. Chaos **08**, 2073 (1998).
[97] E. Freire, E. Ponce, and J. Ros, Limit cycle bifurcations from center in symmetric piecewise-linear systems, Int. J. Bifurcat. Chaos **09**, 895 (1999).
[98] N. Arima, H. Okazaki, and H. Nakano, A generation mechanism of canards in a piecewise linear system, IEICE Trans. Fund. Electron. Commun. Comput. Sci. **E80**, 447 (1997).
[99] S. Coombes, R. Thul, and K. C. A. Wedgwood, Nonsmooth dynamics in spiking neuron models, Physica D **241**, 2042 (2012).
[100] M. Desroches, A. Guillamon, E. Ponce, R. Prohens, S. Rodrigues, and A. E. Teruel, Canards, folded nodes and mixed-mode oscillations in piecewise-linear slow-fast systems, SIAM Rev. **58**, 653 (2016).
[101] M. Desroches, S. Fernández-García, and M. Krupa, Canards in a minimal piecewise-linear square-wave burster, Chaos **26**, 073111 (2016).
[102] S. Fernández-García, M. Desroches, M. Krupa, and E. Teruel, Canard solutions in planar piecewise linear systems with three zones, Dynam. Syst. Int. J. **31**, 173 (2015).
[103] S. Fernández-García, M. Desroches, M. Krupa, and F. Clément, A multiple timescale coupling of piecewise-linear oscillators.

Application to a neuroendocrine system, SIAM J. Appl. Dynam. Syst. **14**, 643 (2015).
[104] A. Roberts, Canard explosion and relaxation oscillation in planar, piecewise-smooth, continuous systems, SIAM J. Appl. Dynam. Syst. **15**, 609 (2016).
[105] A. Kaminaga, V. K. Vanag, and I. R. Epstein, A reaction-diffusion memory device, Angew. Chem. Int. Ed. **45**, 3087 (2006).
[106] P. Goldman-Rakic, Cellular basis of working memory, Neuron **14**, 477 (1995).
[107] K. Wimmer, D. Q. Nykamp, C. Constantinidis, and A. Compte, Bump attractor dynamics in prefrontal cortex explains behavioral precision in spatial working meory, Nat. Neurosci. **17**, 431 (2014).
[108] M. Camperi and X.-J. Wang, A model of visuospatial working memory in prefrontal cortex: Recurrent network and cellular bistability, J. Comput. Neurosci. **5**, 383 (1998).
[109] K. Tornheim, Are metabolic oscillations responsible for normal oscillatory insulin secretion, Diabetes **46**, 1375 (1997).
[110] H. F. Chou, N. Berman, and E. Ipp, Oscillations of lactate released from islets of Langerhans: Evidence for oscillatory glycolysis in beta-cells, Am. J. Physiol. **262**, E800 (1992).
[111] R. Bertram, A. Sherman, and L. Satin, Metabolic and electrical oscillations: Partners in controlling pulsatile insulin secretion, Am. J. Physiol. Endocrinol. Metab. **293**, E890 (2007).
[112] M. J. Merrins, B. Fendler, M. Zhang, A. Sherman, R. Bertram, and L. Satin, Metabolic oscillations in pancreatic islets depend on the intracellular Ca^{2+} level but not Ca^{2+} oscillations, Biophys. J. **99**, 76 (2010).
[113] R. L. Burden and J. D. Faires, *Numerical Analysis* (PWS, Boston, 1980).
[114] R. Kuske and T. Erneux, Localized synchronization of two coupled solid state lasers, Opt. Commun. **139**, 125 (1997).
[115] R. Kuske and T. Erneux, Bifurcation to localized oscillations, Eur. J. Appl. Math. **8**, 389 (1997).
[116] H. G. Rotstein and R. Kuske, Localized and asynchronous patterns via canards in coupled calcium oscillators, Physica D **215**, 46 (2006).
[117] Y. Kuramoto, *Chemical Oscillations, Waves, and Turbulence* (Springer-Verlag, Berlin, 1984).
[118] D. Hansel, G. Mato, and C. Meunier, Clustering and slow switching in globally coupled phase oscillators, Phys. Rev. E **48**, 3470 (1993).
[119] P. Ashwin, G. Orozs, J. Wordsworth, and S. Townley, Dynamics on networks of cluster states for globally coupled phase oscillators, SIAM J. Appl. Dyn. Syst. **6**, 728 (2007).
[120] E. Brown, P. Holmes, and J. Moehlis, Globally coupled oscillator networks, *In Perspectives and Problems in Nonlinear Science: A Celebratory Volume in Honor of Larry Sirovich*, edited by K. Sreenivasan, E. Kaplan, and J. Marsden (Springer, New York, 2003), pp. 183–215.
[121] K. Y. Tsang, R. E. Mirollo, S. H. Strogatz, and K. Wiesenfeld, Dynamics of globally coupled oscillator arrays, Physica D **48**, 102 (1991).
[122] S. H. Strogatz, From Kuramoto to Crawford: Exploring the onset of synchronization in populations of coupled oscillators, Physica D **143**, 1 (2000).
[123] A. Pikovsky and A. Politi, *Lyapunov Exponents: A Tool to Explore Complex Dynamics* (Cambridge University Press, Cambridge, UK, 2016).
[124] A. Birzu and K. Krischer, Resonance tongues in a system of globally coupled oscillators with time-periodic coupling strength, Chaos **20**, 043114 (2010).
[125] M. Somani, M. A. Liwuw, and D. Luss, Evolution and impact of temperature patterns during hydrogen oxidation on a Ni ring, Chem. Eng. Sci. **52**, 2331 (1997).
[126] C. G. Assisi, V. K. Jirsa, and J. A. Kelso, Synchrony and Clustering in Heterogeneous Networks with Global Coupling and Parameter Dispersion, Phys. Rev. Lett. **94**, 018106 (2005).
[127] X. R. Sailer, V. Beato, L. Schimansky-Geier, and H. Engel, Noise-induced effects in excitable systems with local and global coupling, in *Analysis and Control of Complex Nonlinear Processes in Physics, Chemistry and Biology*, edited by L. Schimansky-Geier, B. Fiedler, J. Kurths, and E. Scholl (World Scientific, Singapore, 2007), pp. 1–42.